Cogent Engineering

ISSN: 2331-1916 (Online) Journal homepage: www.tandfonline.com/journals/oaen20

RoboFTOCM: a smart robotic framework for pandemic management in human populations

Kennedy Chinedu Okafor, Omowunmi Mary Longe , Kelvin Anoh , Ijeoma Peace Okafor , Titus Ifeanyi Chinebu & Ikechukwu Ignatius Ayogu

To cite this article: Kennedy Chinedu Okafor, Omowunmi Mary Longe , Kelvin Anoh , Ijeoma Peace Okafor , Titus Ifeanyi Chinebu & Ikechukwu Ignatius Ayogu (2026) RoboFTOCM: a smart robotic framework for pandemic management in human populations, Cogent Engineering, 13:1, 2648925, DOI: 10.1080/23311916.2026.2648925

To link to this article: https://doi.org/10.1080/23311916.2026.2648925

Published online: 16 Apr 2026.

COGENT ENGINEERING
2026, VOL. 13, NO. 1, 2648925
https://doi.org/10.1080/23311916.2026.2648925

BIOMEDICAL ENGINEERING | RESEARCH ARTICLE

OPEN ACCESS Check for updates

RoboFTOCM: a smart robotic framework for pandemic management in human populations

Kennedy Chinedu Okafor[a,b,c,d], Omowunmi Mary Longe[b], Kelvin Anoh[c], Ijeoma Peace Okafor[e], Titus Ifeanyi Chinebu[f] and Ikechukwu Ignatius Ayogu[g]

[a]Department of Engineering, Manchester Metropolitan University, Manchester, UK; [b]Department of Electrical and Electronic Engineering Science, University of Johannesburg, Johannesburg, South Africa; [c]School of Engineering, University of Chichester, Bognor Regis, UK; [d]Department of Management and Entrepreneurship, Imperial College Business School, Imperial College London, London, UK; [e]Department of Public Health, Cardiff Metropolitan University, Llandaff Campus, Cardiff, UK; [f]Department of Applied Sciences, Federal University of Allied Health Sciences, Enugu, Nigeria; [g]Department of Computer Science, Federal University of Technology, Owerri, Nigeria

ABSTRACT

As the human population grows, innovations such as virtual patients, vaccines, biotechnological machines, and microneedles offer solutions to global health crises. Deploying smart robots and support systems can help governments reduce public spending on future respiratory viruses, such as a NextGen Respiratory Virus or NeoCorona Virus. This paper presents a robot-based finite-time optimal control model to combat a hypothetical infectious disease, Pandemic-X, capable of causing a global pandemic. The system is optimised for Pandemic-X, integrating vaccination, robotic control, and incidence-rate dynamics to enhance public health emergency responses. Our approach consolidates optimal control strategies, including vaccination and Computational Internet of Things Robotics (CIoTR), in the post-COVID-19 era. Two strategies are proposed: Pontryagin stochastic optimisation for managing disease spread and a CIoTR-based control approach. The model maximises the susceptible and recovered populations while minimising exposed, asymptomatic, and symptomatic cases. The robot operates in three power modes: i) 'super-active' for high-computation edge inferencing and vaccination, ii) 'moderate' for balanced fallback operations, and iii) 'sleep' for idle states. Results show strong alignment between simulated and real data in vaccination, infection reduction, and hospitalisation trends. These findings demonstrate that robotic optimal control strategies can effectively manage pandemic spread, reduce healthcare burdens, and minimise transmission risk.

ARTICLE HISTORY
Received 30 December 2024
Revised 22 August 2025
Accepted 20 October 2025

KEYWORDS
Medical robotics; computational internet of things; future transmission dynamics; optimal control. Cloud network operating center; marketplace robots

SUBJECTS
Health & Society; Advanced Mathematics; Applied Mathematics; Computation; Computer Engineering; Computer Science (General); Biomedical Engineering

1. Introduction

During the unexpected COVID-19 pandemic in 2019, governments worldwide were compelled to take unprecedented measures and interventions, resulting in massive public spending to protect lives and stabilise economies. For instance, the UK government allocated an astounding £410 billion to combat the COVID-19 pandemic, covering public expenses, business and individual support, and vital NHS operations, including testing and tracing efforts (U.K. Parliament. Commons Library, 2023). Similarly, the US government dedicated an extraordinary $4.6 trillion to help the nation respond to and recover from the pandemic's devastating impact (U.S. Government Accountability Office, 2023). The trend is similar for many wealthy nations. However, many other countries continue to grapple with severe economic challenges, exacerbated by fragile health infrastructures. This highlights the critical need for forward-thinking solutions that not only respond to crises but also fortify defences against future threats. In this context, Pandemic-X represents a proactive anticipation of "the next big disease" before its arrival, enabling

CONTACT Kennedy Chinedu Okafor kennedy.okafor@mmu.ac.uk Department of Engineering, Manchester Metropolitan University, Manchester, M1 5GD, UK

health systems to prepare in advance rather than being caught off guard. This model thus serves as a forward-looking framework for future pandemic preparedness.

Intelligent technological interventions, particularly in robotic science, epidemiology, and control engineering, offer transformative potential in achieving this readiness. By integrating advanced technologies such as Agentic Artificial Intelligence (AI), the Internet of Things (IoT), cloud computing, and robotic sensing systems like Computational Internet of Things Robotics (CIoTR) into healthcare facilities, countries can strengthen their capacity to deliver rapid, effective responses to public health emergencies. This approach also builds resilience, enabling a more proactive and adaptive global health system capable of addressing future crises.

In this work, we shall use CIoTR and RoboFTOCM interchangeably, but these innovations are not merely responses to past shortcomings; they are proactive investments in building a safer, healthier, and more secure future. One notable example is finite-time control design, which has attracted significant attention for its ability to deliver high-precision performance within strict time constraints. This approach has been applied in diverse areas, including micro-robot stabilization (Li et al., 2022; U.K. Parliament. Commons Library, 2023; 5), flux-weakening control systems (Lin et al., 2021), predictive controllers (Lee et al., 2016; Cai et al., 2022; Wang et al., 2022), biological control systems (Liu et al., 2022), robotic manipulator trajectory tracking (Zhang et al., 2022), cooperative control of multi-agent systems (Miao et al., 2023), and state estimation in dynamical systems (Chen et al., 2022).

In general, finite-time stabilisation guarantees that a system's state converges to its desired value within a fixed time frame (Wang et al., 2023). In robotic interventions, this means the system achieves its target state promptly, rather than approaching it asymptotically over an indefinite period. In the context of infectious disease control, effective response often depends on precise mathematical modelling and analysis of epidemic dynamics under high-performance conditions (U.K. Parliament. Commons Library, 2023). Consequently, the application of finite-time optimal control in epidemiological models has gained considerable attention (Wang et al., 2023; Zhai & Xu, 2021). This method offers a detailed understanding of the interactions between key factors in precision disease transmission dynamics, enabling the design of optimal control strategies for pandemic-intelligent healthcare robots (Cao et al., 2024).

Future pandemics involving complex disease conditions, such as COVID-19, can be addressed using controlled robots equipped with Caputo-derivative finite-time control (Huang et al., 2022). When adapted, this approach can enable sophisticated analytical cloning of viruses to support vaccination and control interventions (Eihab & Kailash, 2017; Ketcheson, 2021). The challenge of combating pandemic diseases is immense, and safeguarding the vulnerability of the health sector remains a critical priority.

Complex computational processes are integral to many robotic systems. In medical robotics, for example, DNA cloning' can be used to create multiple identical copies of a specific DNA fragment, such as a gene (Okafor & Longe, 2022). The target gene can be inserted into a plasmid—a circular piece of DNA—through a cloning process aimed at combating infectious diseases via computational transformation (Fang et al., 2020). When combined with computational transformation, DNA cloning demands advanced algorithms and computational biology tools to design, simulate, and optimize the process (Fang et al., 2020). In the post-COVID-19 era, optimising such procedures requires sophisticated computational methods including bioinformatics, machine learning, and compartmental schemes to ensure precision and scalability, helping prevent the re-emergence of similar pandemics.

Various optimal control strategies are employed to understand disease outbreak patterns, assess risks, and implement control measures (Soulaimani & Kaddar, 2023). Compartmental epidemiological models, such as susceptible–infectious–recovered (SIR) and susceptible–exposed–infectious–recovered (SEIR), have been widely used to model COVID-19 spread (Sivadas et al., 2023; Yin et al., 2007; Holst & Licht, 2023; Rey et al., 2023). However, their effectiveness depends on incorporating social dynamics and mixing trends, which vary across countries and demographics. For instance, COVID-19 data from February 14, 2023, showed rising infections in England, Wales, and Scotland, but an unclear trend in Northern Ireland (Escosio et al., 2022). The estimated infection rates were 2.18% in England (1 in 45), 1.79% in Wales (1 in 55), 1.62% in Northern Ireland (1 in 60), and 2.18% in Scotland (1 in 45).

These differences highlight the limitations of traditional SIR and SEIR models in explaining the regional social and demographic variations. Data inconsistencies further complicate control efforts, highlighting the need for localised, context-specific strategy. In this case, an adaptive model that integrate

diverse social, developmental, and epidemiological factors. Hence, precision-driven approaches are essential for effective outbreak management.

Finite-time optimal control framework offers a powerful tool for managing infectious disease spread with greater accuracy and speed. Unlike traditional methods, finite-time stabilisation ensures that control interventions drive the system to the desired state within a fixed time frame, which is critical in our hypothetical future disease. By integrating such control strategies with robotic health interventions, it becomes possible to dynamically adjust responses, optimise vaccination strategies (e.g. via computational cloning techniques), and adapt to the complex social dynamics present in diverse populations. Therefore, the combination of advanced computational biology, precise epidemiological modeling, and finite-time optimal control in intelligent robotic systems forms the backbone of a next-generation pandemic response. This integrated approach not only addresses the shortcomings of past models but also provides robust, and time-guaranteed control architecture capable of protecting public health in a fast-changing world.

In this paper, we apply Pontryagin's Maximum Principle (PMP) separately to two sub-problems: (1) controlling the spread of infection through vaccination and detection strategies, and (2) optimising treatment protocols for symptomatic individuals. Each sub-problem is formulated as a distinct boundary optimisation problem, with its own Hamiltonian and set of parameterised optimality constraints. By integrating transversality and optimality conditions, we establish a point condition on the Hamiltonian and derive backward differential equations governing both the optimal control variables and the adjoint dynamics. Additionally, for practitioners applying optimal control in real-world settings, we provide a specialised formulation targeted to specific deployment scenarios.

While our framework draws on concepts from Joshi et al. (2022), it diverges significantly in key aspects. First, we address a limitation in Hamiltonian differentiation ($\mathcal{H}$), where the Pontryagin Maximum Principle (PMP) cannot be directly applied to *min–max* control models. The Hamiltonian function, which captures the instantaneous change of the system's Lagrangian over time, is central to optimising dynamic systems. This distinction is important because, although PMP can be expressed in continuous time via partial differential models, our approach extends these principles to handle min–max formulations that were not addressed in Joshi et al. (2022).

The work most closely related to ours is Sun et al. (2023); however, we extend it by explicitly addressing uncertainty in system parameters when designing the robotic control model. Our results demonstrate that combining optimal control strategies particularly high vaccination coverage—with intelligent robotic detection significantly reduces the number of exposed and infected individuals. This dual approach slows virus transmission and lowers the incidence of severe illness and hospitalisation, thereby alleviating pressure on healthcare systems. Consequently, the overall risk of COVID-19, including emerging variants, is substantially mitigated. These findings underscore the critical importance of robust vaccination programs and advanced detection technologies in pandemic response. The main contributions of this paper are:

- Constructing optimal control problems to minimize both asymptomatically and symptomatically infected population samples. We develop a Caputo derivative-based finite-time control strategy specifically for intelligent healthcare robots, enabling rapid convergence to desired operational states.
- Implementing PMP-based control variables derived from the Hamiltonian in RoboFTOCM. This enables efficient infection spread management while optimising computational load and adapting to real-world deployment constraints.
- Developing a multi-mode power management system that extends battery life and improves operational sustainability. Our model is supported by sensor correlation analytics for effective control functionality.
- Providing numerical simulations and analytical interpretations to quantify the dynamics of susceptible, exposed, asymptomatically and symptomatically infected, and treated/recovered individuals under optimal and constant control strategies.

The organization of this article is as follows. Section 2 discusses related works on optimal control strategies. Section 3 focuses on the use case scenario for understanding the narratives in the UK. In Section 4, the system model formulation for the transmission dynamics is presented, along with the corresponding computational model derivatives. Section 5 presents the Proof-of-Concept, while Section 6

provides the Numerical simulations. Section 7 presents the results and discussion. Finally, Section 8 concludes the paper and outlines future directions

2. Related works

In this section, we note that while optimal control strategies are pivotal in managing infectious diseases, their full potential remains scarce or underexplored in the real world. The authors (Luo et al., 2024) established analytical strategies for effective pandemic risk-prevention and control. However, their work had a significant gap between theoretical and technological approaches concerning the actual prevention and control efforts. This is because dealing with population uncertainty is at the core of post-COVID-19 risk prediction, prevention, and control strategy. There are a few efforts put in place to fix and control the acceleration of COVID-19. As an example, the use of epidemiological modelling as a control strategy has been explored in Shastri et al. (2020).

Stability conditions for equilibriums within separate malaria and COVID-19 sub-models are derived, revealing global asymptotic stability for COVID-19 equilibria and a potential backward bifurcation for malaria when its reproduction number is less than unity. The combined malaria-COVID-19 model's equilibria are locally stable due to potential backward bifurcation, limiting global stability. Optimal control strategies for both diseases and their co-infection were formulated, utilizing Pontryagin's Maximum Principle to establish their existence and necessary conditions. Also Soulaimani and Kaddar (2023), investigated optimal control of the fundamental SIR epidemic system and outlined policies for an isolation-focused model, a vaccination-centric model, and a combined isolation-vaccination approach. For the COVID-19-specific study, the authors Kokurin et al. (2022) provided a model for epidemics with purely non-pharmaceutical interventions based on an extended SEIR model and optimal control theory. Moreover, the work Lili et al. (2022) investigated optimal COVID-19 epidemic control via social distancing and lockdown measures until the deployment of vaccines. In Gui-Quan et al. (2022), optimal control was used to minimize the number of exposed and infected populations that considered the cost of implementation.

Artificial intelligence (AI) has played a pivotal role in managing the COVID-19 pandemic, particularly in China's context, by aiding healthcare delivery, public sentiment analysis, and epidemic tracking, though ethical concerns around privacy, autonomy, and surveillance remain critical (Ding et al., 2025). Optimal control theory has become essential in infectious disease modeling, allowing policymakers to design effective interventions. The authors of Forrest and Al-Arydah (2025) proposed an SVIR model incorporating behavioral dynamics, demonstrating how caution among the population affects disease transmission and showing the benefits of vaccination and education. The authors of Jain et al. (2025) developed a periodically switched SITR model, adjusting Pontryagin's Maximum Principle to manage treatment and transmission rates in fluctuating conditions. The authors of Afful et al. (2025) introduced a TB–COVID-19 co-infection model and showed that quarantine, vaccination, and prompt treatment can suppress both diseases. Khan and Tanimoto (2025) employed a deterministic SIR-based model to evaluate multiple interventions, finding personal preventive behaviors and ongoing vaccination to be cost-effective. Kamal et al. (2025) used optimal control to assess the social optimum of vaccination strategies, exploring the gap between Nash equilibrium and societal efficiency in the presence of waning immunity. Salwahan et al. (2025) introduced a fractional-order model with vaccination and isolation controls, confirming that fractional optimal control can accurately simulate and mitigate infectious disease spread using real COVID-19 data. Together, these studies highlight the synergy between AI, mathematical modeling, and control theory in managing pandemics while balancing ethical, social, and scientific considerations.

The use of deep learning schemes such as generative Adversarial Networks (GANs) (Rossetti et al., 2023; Coronavirus, 2023), Extreme Learning Machines (ELM) (Kangzhen, 2017), Long/Short Term Memory (LSTM) (Stewart et al., 2020), CovFrameNet (Jamshidi et al., 2020) has been explored in the quest to address control concerns. In Tiago et al. (2023), there have been few examples of realistic, appropriate, and efficient procedures that hospitals have implemented over time. These are based on actual circumstances as well as certain learnings and experiences that incorporate advanced routine epidemic prevention and control. These control strategies have been taken and closely adhered to in most countries to effectively regulate transmission dynamics with complex control challenges. To stop the spread of the

disease, vaccine is needed (Tiago et al., 2023), however, in the absence of the vaccine, people must maintain social distancing as well as any established preventive measures.

Optimal controls are underutilized in managing infectious diseases. For instance, the authors in Mengcan et al. (2021) used medical robots to combat the spread of COVID-19 disease but failed to address co-infection concerns and excluded optimal control models for preventive interventions. In Li et al. (2023), a co-infection model focusing on causal inference analytics was proposed. This explored the dynamic interactions between human response and infectious diseases without applying any control scheme. Introducing the Pontryagin Maximum Principle (PMP) (Oyelade et al., 2021), gives a 1^{st} order boundary condition for co-infection optimality. This is a key component of optimal control theory which is currently applied in various disciplines (Jiang et al., 2022). In context, numerical algorithms use these essential conditions to look for an optimal control point because this can reduce the set of feasible controls into a smaller subset of optimizable control variables, which greatly simplifies the complexity of optimal control. The PMP identifies a pre-condition that an ideal trajectory must satisfy its application in optimal control designs. Hamilton-Jacobi-Bellman optimization scheme/PMP (Di Lallo et al., 2021) is the most widely utilized approach in optimal control.

Recently, studies into the discrete-time PMP with its constraints and geometric boundaries provided a contextual background (Joshi et al., 2022; Sun et al., 2023). The deterministic control model, which is presented as a max optimization problem in which the disturbance is the adversary and seeks to maximize the cost, will be the focus of this paper. This overhead cost is what the infection control strategies seek to minimize. For deterministic/continuous-time models with disturbances, PMPs are useful (Joshi et al., 2022). It is equally useful for systems with parametric perturbations/uncertainties (Sun et al., 2023; Qasem et al., 2024). The min-max control for systems with disturbances has been the subject of extensive research in the game-theoretic paradigm for continuous-time systems (Guo, 2023).

Numerous researchers have used optimal control theory to explore compartmental architectures and process diagrams within epidemiology research domain. For instance Kipka and Gupta (2019), focused on determining the most effective approach to balance vaccination and treatment strategies within variations of standard SIR, SIRS, and SEIR epidemiological models, aiming to minimize the number of infected individuals. In Phogat et al. (2018), an age-specific SIR model was introduced for susceptible, vaccinated, infected, and recovered (SVIR) also known as a susceptible–infected–recovered model. The authors illustrated how susceptible and infected individuals interact within a community while examining the model using other optimal control theory concepts and mathematical analysis. The authors Athawale et al. (2023) investigated the transmission dynamics of brucellosis in Jilin province in China, an area significantly affected by the disease.

The authors of Jiang et al. (2023) and Yang et al. (2023) focused on a specific category of methods aimed at finding approximate solutions for noisy, nonlinear, and irregular operator equations in a Hilbert space for a COVID-19 SEIR-like model. Their use of iterative approach for parameter identification involves a regularization technique and incorporates a stopping rule dependent on the error level present in the input data. In Zaman et al. (2017), the authors formulated the SIR epidemic model to understand disease spread patterns and introduced a recovery rate control for pattern manipulation. In Ma et al. (2022), the authors focused on a diffusive model for foot-and-mouth disease (FMD) while investigating the transmission dynamics and control measures. Kokurin et al. (2022) presented a mathematical model addressing the co-dynamics of malaria and COVID-19. Despite advances in modeling infectious diseases and co-infections, optimal control strategies—particularly those leveraging PMP and related methods remain underutilised or partially applied, limiting their full potential in guiding effective, integrated disease intervention policies.

3. Use case scenario

In this section, we shall focus the analysis on three major trends from Office for National Statistics (ONS) namely (Escosio et al., 2022): COVID-19 infection rate changes by region, distribution of COVID-19 variants, and COVID-19 infection rates by age group in England. We then analyze the effectiveness of COVID-19 control efforts in England, Wales, Northern Ireland, and Scotland, using data from the UK Office of National Statistics (Escosio et al., 2022) as an example. Official estimates, calculated using

modeled data, reveal a significant trend of weaknesses in control strategies, as evidenced by a Cronbach Alpha test score of 0.95, indicating high internal consistency. The model, which is updated weekly to incorporate new test results, identifies trends in infection rates.

As shown in Figure 1, as of the week ending February 14, 2023, there was an increase in COVID-19 infections in England (2.18%), Wales (1.79%), and Scotland (2.18%). In Northern Ireland, the trend was less clear, with an infection rate of 1.62%. Since late June 2022, most COVID-19 infections in the UK have been attributed to the Omicron variant BA.5 and its sub-lineages. However, by mid-January 2023 in Figure 2, variants such as BA.2.75 and its sub-lineages including XBB, CH.1.1, and their sub-lineages, had become more prevalent. Specifically, in the week ending February 12, 2023, the BA.2.75 sub-lineages CH.1.1 and XBB accounted for 32.2% and 40.3% of all sequenced cases, respectively, while the Omicron BQ.1 variant (a sub-lineage of BA.5) was responsible for 19.8% of sequenced cases. In England, for the week ending February 12, 2023, in Figure 3, infection rates increased among individuals over 25 years old but decreased among children from kindergarten through grade 11. Trends for those aged 12–24 were ambiguous, with greater uncertainty in age group estimates compared to the overall data for England. Control measures such as vaccinations, social distancing, and lockdowns are being evaluated for their effectiveness against emerging variants. The findings underscore the need for a robust computational approach that can be further validated through advanced clinical trials.

To optimise interventions based on the data, we propose targeted strategies for each scenario:

Case 1: In England and Scotland, focus on intensified testing, contact tracing, targeted restrictions, enhanced public health messaging, and vaccination campaigns due to higher infection rates (see Figure 1).

Case 2: As shown in Figure 2, target public health and vaccination strategies to combat prevalent XBB variants by developing targeted vaccines or boosters, monitoring treatment effectiveness, and adjusting policies as needed.

Case 3: Based on Figure 3, prioritise booster vaccinations and outreach for older adults with rising infections, maintain preventive measures for children and adolescents, and monitor the 12–24 age group to adapt strategies as trends emerge.

We now explain the relevance of our system model formulation below.

- First, by focusing on maximising critical control parameters, our approach ensures that the most influential factors in controlling disease transmission such as testing frequency, contact tracing efficiency, targeted restrictions, and vaccination rates are optimised. This directly supported the implementation of intensified testing, effective contact tracing, and enhanced vaccination campaigns.
- Computational Stability Constraints is another benefit. Our approach offers computational stability. This means that the proposed strategies are not only effective but also practical and reliable over time. This is crucial for maintaining long-term interventions such as localized lockdowns, age-specific

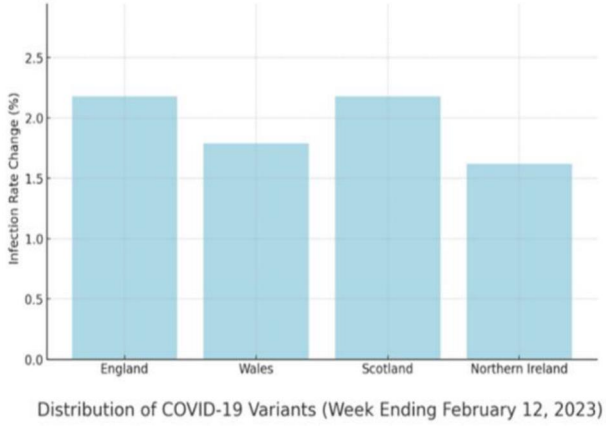

Figure 1. COVID-19 infection rate changes by region (Data source: ONS, 2023).

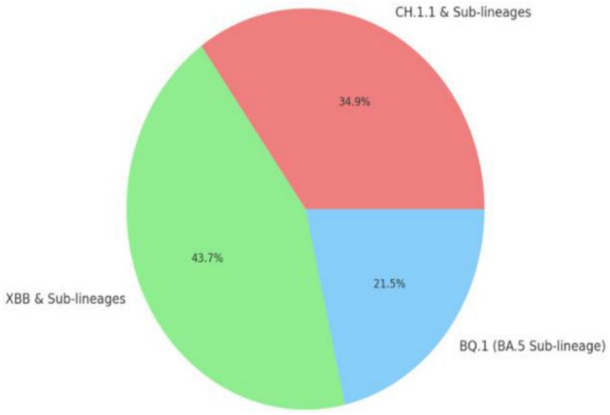

Figure 2. Distribution of COVID-19 variants, week ending February 12, 2023 (Data source: ONS, 2023).

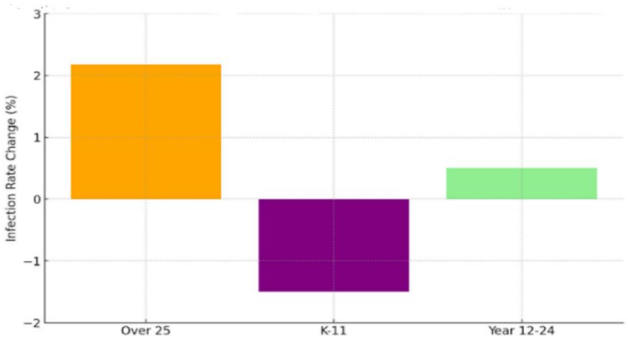

Figure 3. COVID-19 infection rates by age group in England (Data source: ONS, 2023).

vaccination drives, and monitoring evolving variants like XBB. It ensures that the strategies remain feasible and sustainable as conditions change.

- Pontryagin's Maximum Principle (PMP) is used to formulate a stochastic optimization problem. A mathematical framework was used to identify the best possible control strategies given uncertain conditions. The optimised parameters ensure computational stability. The adapted strategies are based on real-time data and stochastic conditions.

4. System model formulation

To enhance the control strategy for the transmission dynamics, we focused on maximising critical control parameters while ensuring computational stability constraints in RoboFTOCM. Our optimal control strategy is formulated based on the PMP stochastic optimisation problem discussed in Section 2. The details of the mathematical properties are summarised in Table 1.

4.1. Assumptions

We consider a small subset of a large population prone to Pandemic-X, exhibiting symptoms such as catarrh, cough, sore throat, fever, chest pain, occasional breathing difficulty, and malaise. Asymptomatic individuals show no symptoms, while symptomatic individuals experience noticeable—but not precisely measurable—disease effects.

The larger population is mostly free of Pandemic-X and serves as a steady source of both vaccinated and unvaccinated exposed individuals. Exposed individuals who become infectious are classified into two groups: infected with symptoms and infected without symptoms, with the latter assumed to be less infectious. Our study focuses on this sample population within human society. Using Figure 1, the density of Pandemic-X cases detected by the CIoT robot can be calculated. This robot acts as an intelligent system, gathering information from its environment and performing tasks with optimised reliability based on inferred knowledge. Table 1 lists the variables related to the Pandemic-X CIoTR environment

Table 1. Summary of notation I.

Variable	Description
Pandemic-X	Any strain of pandemic-X variant k
R_{0A}	Basic reproduction number of the asymptomatically infected
R_{0I}	Basic reproduction number of the symptomatically infected
R_{CR}	Effective basic reproduction number of the model (Both Asymptomatically and symptomatically infected)
$S(t)$	Susceptible individuals (those who are at risk of contracting Pandemic-X infection)
$V(t)$	Vaccinated individuals against Pandemic-X infection
$E(t)$	Exposed individuals against Pandemic-X infection
$A(t)$	Infectious individuals without Pandemic-X infection symptoms
$I(t)$	Infectious individuals with Pandemic-X infection symptoms
$H(t)$	Isolated/hospitalized Individuals who are detected with Pandemic-X infection
$T(t)$	Treated and recovered Individuals from Pandemic-X infection
$R(t)$	Robotic compartment

(baseline robotics control), while Table 2 details the parameters and descriptions for the Pandemic-X infection model.

We incorporate a saturated incidence rate and robotic control alongside vaccination in the Pandemic-X infection model to build a more realistic and effective framework for controlling virus spread. The saturated incidence rate captures the non-linear dynamics of Pandemic-X transmission, providing a precise representation of how the disease spreads. Robotic control evaluates intervention effectiveness in reducing infections, especially where human contact must be minimized. Vaccination accounts for immunity effects, improving predictions of outbreak trends and campaign impacts. Together, these elements form a comprehensive model that captures the complex interactions between human behaviour, technology, and biology to better guide public health strategies against Pandemic-X.

4.2. Optimisation model formulation

To derive our optimisation engine for control parameters of infectious diseases in a scalable population, we used Figure 4 as a compact architecture. Now, the mathematical representation of the model is given by the system of nonlinear differential equations in (1a):

$$\left.\begin{aligned}
\frac{dS(t)}{dt} &= \varphi(1-\eta) + \varpi V(t) + \theta T(t) - \left(\mu + \omega + \beta\left(\frac{I(t)}{1+\alpha_1 I} + \frac{\rho A(t)}{1+\alpha_2 I}\right)\right)S(t)\\
\frac{dV(t)}{dt} &= \eta\varphi + \tau\varrho E(t) + \omega S(t) - (\mu+\varpi)V(t)\\
\frac{dE(t)}{dt} &= \beta\left(\frac{I(t)}{1+\alpha_1 I} + \frac{\rho A(t)}{1+\alpha_2 I}\right)S(t) - \left(\mu + \tau\varrho + \upsilon R(t) + \varrho + \emptyset\right)E(t)\\
\frac{dA(t)}{dt} &= \emptyset\varepsilon E(t) - (\mu + \sigma R(t))A(t)\\
\frac{dI(t)}{dt} &= \emptyset(1-\varepsilon)E(t) - (\mu + \kappa + \gamma R(t))I(t)\\
\frac{dH(t)}{dt} &= (\upsilon E(t) + \sigma A(t) + \gamma I(t))R(t) - (\mu + \Delta + \xi)H(t)\\
\frac{dT(t)}{dt} &= \xi H(t) + \varrho E(t) - (\mu+\theta)T(t)\\
\frac{dR(t)}{dt} &= \psi\zeta - \delta R(t)
\end{aligned}\right\} \tag{1a}$$

where,

$$\zeta = \Lambda e^{-t(\pi-\hat{\pi})} \tag{1b}$$

ψ is the recruitment rate of robots, ζ is the effective performance rate of the robot and δ is the robot performance breakdown rate.

Table 2. Summary of notation II.

Parameter	Description
$\varphi(1-\eta)$	Recruitment rate into the susceptible compartment
$\varphi\eta$	Recruitment rate into the vaccinated compartment
ω	Vaccination rate of the susceptible population
ϖ	Waning rate of vaccine
β	Effective contact rate
α_1	Parametric measure for psychological or inhibitory effect ($E(t)$ to $I(t)$)
ρ	The modified factor for the Pandemic-X infectious individuals without symptoms
α_2	Inhibitory effect ($E(t)$ to $A(t)$)
μ	Natural death rate
$\tau\varrho$	Recovery-rate of exposed persons ready for immune response, but were subsequently moved to the recovered compartment
ϱ	Recovery-rate of exposed persons ready for immune response, who were not vaccinated but were moved to recovered
$\emptyset(1-\varepsilon)$	Rate at which the exposed become infectious with symptoms
$\emptyset\varepsilon$	Rate at which the exposed become infectious without symptoms
υ	Isolation/Hospitalization rate of the exposed (infected) individuals after effective detection by Stream Robot.
σ	Isolation/Hospitalization rate of the infectious without symptoms after effective detection by Stream Robot.
γ	Isolation/Hospitalization rate of the infectious with symptoms after effective detection by Stream Robot.
κ	Death rate of the infectious with symptoms due to the Pandemic-X infection.
Δ	Death rate of the Isolation/Hospitalization due to the Pandemic-X infection
ξ	Recovery rate after treatment from Pandemic-X infection
θ	Rate at which the treated who recovered move to the susceptible compartment
ψ	Recruitment rate of Robot
ζ	Effective performance rate of the Robot
δ	Robot performance breakdown rate
π	Distance at which the data is generated by the Robot and battery life
$\hat{\pi}$	Half of the distance and battery life understudy
t	The time

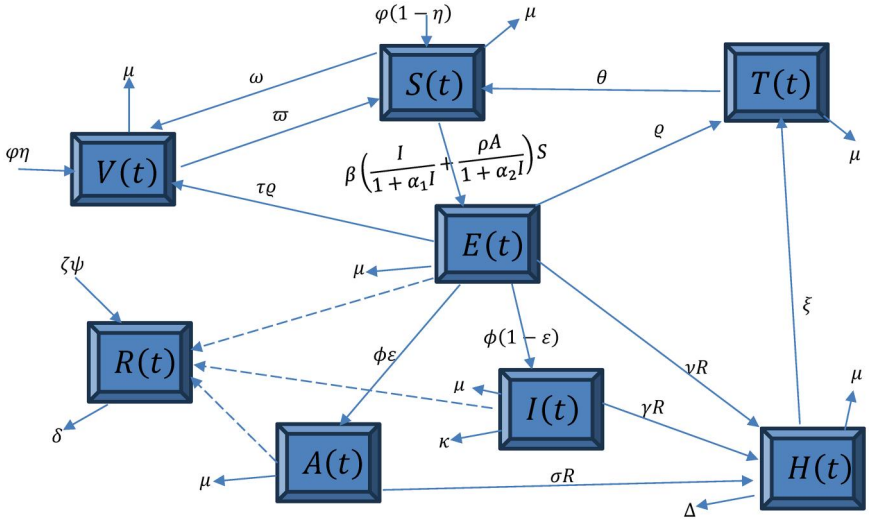

Figure 4. Optimisation control flow diagram for pandemic-X dynamics.

The possible generation of data by the robot per individual, *id* denoted by Λ and, t is the time. π represents the distance at which the data is generated by the robot and battery life while, $\hat{\pi}$ represents half of the distance and battery life understudy.

Let the human population be given by $N_1(t)$ at time t. This may be fundamentally separated into seven (7) mutually exclusive compartments of individuals described below.

- First, those who have not come in contact with Pandemic-X infected individuals but are at risk of being infected with Pandemic-X infection, denoted by $S(t)$ (Susceptible individuals).
- The second compartment is individuals who have received vaccination against Pandemic-X infection, denoted by $V(t)$ (Vaccinated individuals);
- Third, there are non-vaccinated individuals who were exposed to Pandemic-X infection, but subsequently may become infected. This set is denoted by $E(t)$ (Exposed individuals);
- The fourth set is individuals infected without symptoms, i.e., denoted by $A(t)$ (Asymptomatic individuals);

- The fifth set is individuals infected with symptoms, i.e., denoted by $I(t)$ (symptomatic individuals).
- The sixth group is individuals infected with Pandemic-X infection and isolated for treatment in the hospital. This group is denoted with $H(t)$ (Isolated/hospitalised individuals)
- The seventh group is individuals who recovered after treatment, i.e., denoted by $T(t)$ (Treated/recovered individuals). In context, both the exposed, infected without symptoms, and infected with symptoms are detected by the CIoT robotic control system to reduce the rate of transmission due to contact. This is denoted by $R(t)in$ RoboFTOCM.

4.3. Control computational architecture

The compartmental architecture in Figure 4 shows the flow structure of individuals in a sample population with the possibility of acquiring Pandemic-X at time *t*. The design framework is derived from our earlier work (Okafor et al., 2025). We use the following assumptions to achieve the optimisation objective for RoboFTOCM.

- Mixing between people happens in a uniform way (i.e., compact homogeneity attribute).
- Only the exposed compartment after infection produces the population of people with either symptomatic or asymptomatic Pandemic-X infection.
- Exposed individuals who may not be infectious may acquire some immunity through vaccination and this reduces the risk of subsequent infection.
- Additionally, it is hypothesized that exposed persons develop some immunity because of the infection, which lowers the chance of re-infection but does not completely shield them against contracting Pandemic-X infection.
- The acquired vaccine-induced immunity of the vaccinated people may deteriorate with time. It is believed that Pandemic-X *infected* people spread the infection at a rate of λ.
- Susceptible individuals who have never been successfully vaccinated acquire infection with Pandemic-X *while* those whose protective effect of vaccination has worn off move back to the susceptible compartment.

Considering Figure 4, the representation of the human population is therefore given as:

$$N_1(t) = S(t) + V(t) + E(t) + A(t) + I(t) + H(t) + T(t) \tag{2a}$$

While the robotic population is given as

$$N_2(t) = R(t) \tag{2b}$$

Thus, the entire population sample is given as

$$N(t) = N_1(t) + N_2(t) \tag{3}$$

$$N(t) = S(t) + V(t) + E(t) + A(t) + I(t) + H(t) + T(t) + R(t) \tag{4a}$$

$$N(t) = \sum_{i=1}^{8} N(t) \tag{4b}$$

where i =1, 2, 3, …, 8,

But following effective contact with symptomatic and asymptomatic infection at rate λ, (5) is now given as the infectious force associated with Pandemic-X infection.

$$\lambda = \beta\left(\frac{I}{1+\alpha_1 I} + \frac{\rho A}{1+\alpha_2 I}\right) \tag{5}$$

where β is the effective contact rate for Pandemic-X infection (contact sufficient to result in Pandemic-X infection) and the modification parameter $\rho \geq 1$ accounts for the relative infectiousness of individuals with asymptomatic Pandemic-X, where $\frac{1}{1+\alpha_1}$ and $\frac{1}{1+\alpha_2}$ capture the inhibitory effect from the attitudinal change found in susceptible persons at the instance of increase from the crowded effect found in persons infected already.

4.4. Model analysis

- **Positivity and Well-Posedness of the Model**

Given that our model tracks Pandemic-X infection transmission as an example, we then focus on how the Stream Robots detects infected individuals, it's essential to ensure that all state variables stay non-negative. Since the population under study consists of physical quantities that cannot be negative, we must prove that these variables are non-negative for all time (t).

To make the model (1a) both epidemiologically and mathematically valid, we demonstrate that the solution to the model (1a) with positive initial data remains positive for all $t \geq 0$. Therefore, we ensure the model's consistency and reliability in representing real-world scenarios.

Lemma 1: *The Physically Feasible Region*

$$\mathcal{D} = \left\{ (S(t) + V(t) + E(t) + A(t) + I(t) + H(t) + T(t) + R(t)) \epsilon \mathbb{R}_+^8 : N_1 \leq \frac{\varphi}{\mu}; N_2 \leq \frac{\psi\zeta}{\delta} \right\}$$

Proof: Notice from (2a) that $\mathcal{D}$ is a positively invariant set for model system (1a) since adding the first seven sub-equations, that is,

$$N_1(t) = S(t) + V(t) + E(\mathrm{t}) + A(t) + I(t) + H(t) + T(t)$$

$$\frac{dN_1(t)}{dt} = \varphi - \mu(S(t) + V(t) + E(t) + A(t) + I(t) + H(t) + T(t)) - \Delta H(t) - \kappa I(t) \tag{6}$$

But at COVID-19 infection free equilibrium, $\Delta H(t) = \kappa I(t) = 0$

$$\frac{dN_1(t)}{dt} = \varphi - \mu N_1(t) \tag{7}$$

And so $\frac{dN_1(t)}{dt} < 0$ if $N_1(t) > \frac{\varphi}{\mu}$. Thus, from system (7) and Gronwell's inequality, it follows that

$$N_1(t) \leq N_1(0)e^{-\mu t} + \frac{\varphi}{\mu}(1 - e^{-\mu t}) \tag{8}$$

$$0 \leq N_1 \leq \frac{\varphi}{\mu} \ as \ t \longrightarrow \infty \tag{9}$$

Therefore, $N_1(t) \leq \frac{\varphi}{\mu}$ provided $N_1(0) \leq \frac{\varphi}{\mu}$. Hence, $\mathcal{D}$ is a positively invariant set and therefore the model is well-posed both mathematically and epidemiologically. Thus, the dynamic flow of the model can sufficiently be considered in $\mathcal{D}$.

4.5. Optimal control objective function

The optimal control theory used to develop the proposed composite control strategy is obtained from Tchoumi et al. (2021) and Kantner and Koprucki (2020). The interest is to achieve the Pandemic-X infection transmission dynamics by maximizing the number of susceptible $S(t)$ and treated/Recovered $T(t)$; minimizing the number of exposed $E(t)$, asymptomatically infected $A(t)$ and symptomatically infected $I(t)$ in the population. We also minimize the costs required to control Pandemic-X infections by using the time-dependent control variable Vaccination $u_1(t)$ of the susceptible individuals, robotic identification $u_2(t)$ of the exposed, asymptomatically infected, and symptomatically infected, and effective treatment $u_3(t)$ Isolated/Hospitalized and they are bounded Lebesgue integral function (Iacoviello & Stasio, 2013).

In this case, we constructed the optimal control problem designed to minimize the objective function given in (24) and (25). This is not directly related to the convection control variables, and cost functions.

$$\textbf{\textit{Min}}\{\mathcal{J}(u_1, u_2, u_3)\} = \int_0^{t_f} \left[B_1 S(t) + B_2 E(t) + B_3 A(t) + B_4 I(t) + \frac{1}{2}\left(C_1 u_1^2 + C_2 u_2^2 + C_3 u_3^2\right) \right] dt \tag{10}$$

Subject to

$$\left.\begin{aligned}
\frac{dS(t)}{dt} &= \varphi(1-\eta) + \varpi V(t) + \theta T(t) - \left(\mu + u_1(t) + \beta(1-u_2(t))\left(\frac{I(t)}{1+\alpha_1 I} + \frac{\rho A(t)}{1+\alpha_2 I}\right)\right)S(t)\\
\frac{dV(t)}{dt} &= \eta\varphi + \tau\varrho E(t) + u_1(t)S(t) - (\mu+\varpi)V(t)\\
\frac{dE(t)}{dt} &= \beta(1-u_2(t))\left(\frac{I(t)}{1+\alpha_1 I} + \frac{\rho A(t)}{1+\alpha_2 I}\right)S(t) - \left(\mu + \tau\varrho + u_2(t)R(t) + \varrho + \emptyset\right)E(t)\\
&\quad -(u_1(t)+u_3(t))E(t)\\
\frac{dA(t)}{dt} &= \emptyset\varepsilon E(t) - (\mu + u_2(t)R(t))A(t) - (u_1(t)+u_3(t))A(t)\\
\frac{dI(t)}{dt} &= \emptyset(1-\varepsilon)E(t) - (\mu+\kappa+u_2(t)R(t))I(t) - (u_1(t)+u_3(t))I(t)\\
\frac{dH(t)}{dt} &= u_2(t)(E(t)+A(t)+I(t))R(t) - (\mu+\Delta+u_3(t))H(t)\\
\frac{dT(t)}{dt} &= u_3(t)H(t) + \varrho E(t) - (\mu+\theta)T(t) + (u_1(t)+u_3(t))(E(t)+A(t)+I(t))\\
\frac{dR(t)}{dt} &= \psi\zeta - \delta R(t)
\end{aligned}\right\} \tag{11}$$

With initial conditions, $S(0)\geq 0, V(0)\geq 0, E(0)\geq 0, A(0)\geq 0, I(0)\geq 0, H(0)\geq 0, T(0)\geq 0, R(0)\geq 0$.

In (10), B_1, B_2, B_3 *and* B_4 represent the weight constant of the susceptible, exposed, asymptomatically infected, and symptomatically infected individuals respectively. Similarly, in the objective functional C_1, C_2 *and* C_3 are the weight constant for the vaccination, robotic identification of the exposed, asymptomatically infected, symptomatically infected, and treatment control. The terms $\frac{1}{2}C_1u_1^2$, $\frac{1}{2}C_2u_2^2$ *and* $\frac{1}{2}C_3u_3^2$ describes the cost associated with vaccination, robotic identification, and treatment at time t, t_f being the final time. Due to the boundedness of the state and adjoint functions and the Lipschitz structure of the ordinary differential equations (ODEs), we achieved the uniqueness of the optimal control pair, consistent with the optimality system (Iacoviello & Stasio, 2013; Zaman et al., 2008; Zaman et al., 2009; Jafarimoghaddam & Soler, 2023; Jung et al., 2002).

Proposition I: *There exists a unique solution to the initial value problem in (10) provided that the optimal control pair uniqueness is satisfied.*

Proof of Proposition I

In context, we seek the optimal controls u_1^*, u_2^*, u_3^* such that.

$$\mathcal{J}\left(u_1^*, u_2^*, u_3^*\right) = \min_{u_1, u_2, u_3 \in W} \mathcal{J}(u_1, u_2, u_3) \tag{12}$$

Subject to system (54) where W is the set f admissible control that is Lebesgue measurable time-dependent function on $[0,1]$ defined by

$$W = \left\{u_1, u_2, u_3 : 0 \leq u_{i\ \min} \leq u_i(t) \leq u_{i\ \max} \leq 1, i = 1,2,3,; t \in [0, t_f]\right\} \tag{13}$$

With PMP (Joshi et al., 2022; Richard et al., 2021; Bongard, 2008) applied while offering required conditions for full scaled optimal control problem, Pandemic-X infection model (11) with (10) and (12) will be converted into Hamiltonian, $\mathcal{H}$, point wisely with respect to u_1, u_2, u_3, thus, yielding (14). The right-hand side (RHS) of (14) captured f_i as shown below.

$$\mathcal{H} = B_1S(t) + B_2E(\mathrm{t}) + B_3A(t) + I(t) + \frac{1}{2}\left(C_1u_1^2 + C_2u_2^2 + C_3u_3^2\right) + \sum_{i=1}^{8}\lambda_i f_i \ ; i = 1, \ldots, 8 \tag{14}$$

where f_i is the RHS mapping of the differential system of *ith* state variables. Expanding (14) yields

$$\begin{aligned}\mathcal{H} &= B_1S(t) + B_2E(t) + B_3A(t) + I(t) + \frac{1}{2}\left(C_1u_1^2 + C_2u_2^2 + C_3u_3^2\right)\\ &+ \lambda_1\left(\varphi(1-\eta) + \varpi V(t) + \theta T(t) - \left(\mu + u_1(t) + \beta(1-u_2(t))\left(\frac{I(t)}{1+\alpha_1 I} + \frac{\rho A(t)}{1+\alpha_2 I}\right)\right)S(t)\right)\\ &+ \lambda_2\left(\eta\varphi + \tau\varrho E(t) + u_1(t)S(t) - (\mu+\varpi)V(t)\right)\\ &+ \lambda_3\left(\beta(1-u_2(t))\left(\frac{I(t)}{1+\alpha_1 I} + \frac{\rho A(t)}{1+\alpha_2 I}\right)S(t) - \left(\mu + \tau\varrho + u_2(t)R(t) + \varrho + \emptyset\right)E(t)\right) - (u_1(t)+u_3(t))E(t)\\ &+ \lambda_4(\emptyset\varepsilon E(t) - (\mu + u_2(t)R(t))A(t) - (u_1(t)+u_3(t))A(t))\\ &+ \lambda_5\left(\emptyset(1-\varepsilon)E(t) - (\mu+\kappa+u_2(t)R(t))I(t) - (u_1(t)+u_3(t))I(t)\right)\\ &+ \lambda_6(u_2(t)(E(t)+A(t)+I(t))R(t) - (\mu+\Delta+u_3(t))H(t))\\ &+ \lambda_7\left(u_3(t)H(t) + \varrho E(t) - (\mu+\theta)T(t) + (u_1(t)+u_3(t))(E(t)+A(t)+I(t))\right) + \lambda_8\left(\psi\zeta - \delta R(t)\right)\end{aligned} \tag{15}$$

By introducing PMP alongside with existence result mapped for control pairs from (12), proposition 1 is resolved.

Proposition 2: *Consider an optimal control pairs* (u_1^*, u_2^*, u_3^*) *and corresponding solution* $\hat{S}, \hat{V}, \hat{E}, \hat{A}, \hat{I}, \hat{H}, \hat{T}, \hat{R}$ *that maximizes* $\mathcal{J}(u_1, u_2, u_3)$ *over* W, *then there exists an adjoint variable.*$\lambda_1(t), \lambda_2(t), \lambda_3, +\lambda_4(t), \lambda_5(t), \lambda_6(t), \lambda_7(t), \lambda_8(t)$ *satisfying*

$$\left.\begin{aligned}\frac{d\lambda_1}{dt} &= -B_1 + \beta\left(1-u_2^*\right)\left(\frac{\hat{I}}{1+\alpha_1\hat{I}} + \frac{\rho\hat{A}}{1+\alpha_2\hat{I}}\right)(\lambda_1-\lambda_3) + u_1^*(\lambda_1-\lambda_2) + \mu\lambda_1\\ \frac{d\lambda_2}{dt} &= \mu\lambda_2 + \varpi(\lambda_2-\lambda_1)\\ \frac{d\lambda_3}{dt} &= -B_2 + \mu\lambda_3 + \tau\varrho(\lambda_3-\lambda_2) + u_2^*\hat{R}(\lambda_3-\lambda_6) + \varrho(\lambda_3-\lambda_7) + \emptyset\lambda_3 - \emptyset\varepsilon\lambda_4 - \emptyset(1-\varepsilon)\lambda_5\\ &\quad +(u_1^*+u_3^*)(\lambda_3-\lambda_7)\\ \frac{d\lambda_4}{dt} &= -B_3 + \frac{\rho\hat{S}}{1+\alpha_2\hat{I}}(\lambda_1-\lambda_2) + \mu\lambda_4 + u_2^*\hat{R}(\lambda_4-\lambda_6) + \left(u_1^*+u_3^*\right)(\lambda_4-\lambda_7)\\ \frac{d\lambda_5}{dt} &= -B_4 + \frac{\hat{S}}{\left(1+\alpha_1\hat{I}\right)^2}(\lambda_1-\lambda_2) + \mu\lambda_5 + \kappa\lambda_5 + u_2^*\hat{R}(\lambda_5-\lambda_6) + \left(u_1^*+u_3^*\right)(\lambda_5-\lambda_7)\\ \frac{d\lambda_6}{dt} &= \mu\lambda_6 + \Delta\lambda_6 + u_3^*(\lambda_6-\lambda_7)\\ \frac{d\lambda_7}{dt} &= \mu\lambda_7 + \theta(\lambda_7-\lambda_1)\\ \frac{d\lambda_7}{dt} &= \delta\lambda_8\end{aligned}\right\} \tag{16}$$

With transversality condition

$$\lambda_1(t) = \lambda_2(t) = \lambda_3(t) = \lambda_4(t) = \lambda_5(t) = \lambda_6(t) = \lambda_7(t) = \lambda_8(t) = 0 \tag{17}$$

and optimality condition is given by

$$\left.\begin{aligned}u_1^*(t) &= \frac{\omega\hat{S}((\lambda_1-\lambda_2))}{C_1}\\ u_2^*(t) &= \frac{\upsilon\hat{E}\left((\lambda_3-\lambda_6)\hat{R}\right) + \sigma\hat{A}\left((\lambda_4-\lambda_6)\hat{R}\right) + \gamma\hat{I}\left((\lambda_5-\lambda_6)\hat{R}\right)}{C_2}\\ u_3^*(t) &= \frac{\xi\hat{H}((\lambda_1-\lambda_2))}{C_3}\end{aligned}\right\} \tag{18}$$

Proof of Proposition 2

The differential system model in (16) is gotten through the differentiation of the Hamiltonian function, $\mathcal{H}$. The evaluation at the optimal control frame yields

$$\left.\begin{aligned} -\frac{d\lambda_1}{dt} &= \frac{\partial \mathcal{H}}{\partial \hat{S}}, \lambda_1(t_f) = 0; \\ &\vdots \\ -\frac{d\lambda_8}{dt} &= \frac{\partial \dot{\mathcal{H}}}{\partial \hat{R}}, \lambda_8(t_f) = 0 \end{aligned}\right\}$$

By equating to zero, the derivatives of Hamiltonian for the control variables found its set W, is given by

$$\frac{\partial \mathcal{H}}{\partial u_1^*} = 0, \frac{\partial \mathcal{H}}{\partial u_2^*} = 0 \ \textit{and} \ \frac{\partial \mathcal{H}}{\partial u_3^*} = 0$$

We solve $u_1(t) as\ u_1^*(t), u_2(t) as\ u_2^*(t) and\ u_3(t) as\ u_3^*(t)$ to obtain

$$\left.\begin{aligned} u_1^*(t) &= \frac{\omega \hat{S}((\lambda_1 - \lambda_2))}{C_1} \\ u_2^*(t) &= \frac{\upsilon \hat{E}\left((\lambda_3 - \lambda_6)\hat{R}\right) + \sigma \hat{A}\left((\lambda_4 - \lambda_6)\hat{R}\right) + \gamma \hat{I}\left((\lambda_5 - \lambda_6)\hat{R}\right)}{C_2} \\ u_3^*(t) &= \frac{\xi \hat{H}((\lambda_1 - \lambda_2))}{C_3} \end{aligned}\right\} \tag{19}$$

By leveraging the control boundary state, we then divide the optimality conditions into

$$\begin{aligned} u_1^*(t) &= \max\left\{0, \min\left\{1, \frac{\omega \hat{S}((\lambda_1 - \lambda_2))}{C_1}\right\}\right\} \\ u_2^*(t) &= \max\left\{0, \min\left\{1, \frac{\upsilon \hat{E}\left((\lambda_3 - \lambda_6)\hat{R}\right) + \sigma \hat{A}\left((\lambda_4 - \lambda_6)\hat{R}\right) + \gamma \hat{I}\left((\lambda_5 - \lambda_6)\hat{R}\right)}{C_2}\right\}\right\} \\ u_3^*(t) &= \max\left\{0, \min\left\{1, \frac{\xi \hat{H}((\lambda_1 - \lambda_2))}{C_3}\right\}\right\} \end{aligned} \tag{20}$$

4.6. Computational complexity algorithm

The complexity of Algorithm I stems from the joint optimization in (10) under the constraints in (11). To address computational complexity (CC), the joint model in (11) can be decomposed into two subproblems: admission control and resource management. In this case, the other subproblems are solved combinatorially. A clear analysis of (11) supports the optimal decomposition addressed by Algorithm I. The optimal control sub-problem derives the density boundary data admissible to the robotic engine, using queue-based reference baselines. Meanwhile, the resource optimality sub-problem identifies the optimal control allocation based on the current state. As shown in Algorithm I, the CC in each time slot is dominated by the iterative procedure from steps 7 to 13. The best epoch in terms of reduced memory and CPU gives the CC of next $(i+1)$ cycle as *O(RMC)*. The LaGrange-multiplier μ uses $\vartheta\left({}^{1}/_{\varepsilon^2}\right)$ iterations to the expected state of the optimal control objective policy. Hence, Algorithm I offer practical implementation.

Algorithm I. Optimal Control Objective Policy

1: **Input:**

$$S(t); V(t); E(t); A(t); I(t); H(t); T(t), \lambda, \beta,$$

Output: $\eta, \omega, \upsilon, \sigma$ *and* γ

$$\textbf{\textit{Min}}\{\mathcal{J}(u_1, u_2, u_3)\}$$

Parameters: $W \leftarrow$Empty; // $\mathcal{J}(u_1^*, u_2^*, u_3^*)$ weighted Moving Average
Optimal weight$\leftarrow$0; *weighted Moving*$\leftarrow$0; *total Weight*$\leftarrow$0;
$u_1^*, u_2^*, u_3^* \leftarrow$0; *fiboB*$\leftarrow$1;
W historyItem$\leftarrow$ null; //
int *i*$\leftarrow$0; *t*$\leftarrow$0; Q(0) $\leftarrow$ 0, *W*

While $i < \mathcal{H}$ *d* ***do***
  $\hat{S}, \hat{V}, \hat{E}, \hat{A}, \hat{I}, \hat{H}, \hat{T}, \hat{R} \leftarrow$HistoryList.get (HistoryList.*Size*()–monitorCallSchedule–*i*)
  $\lambda_1(t)$*_weight*$\leftarrow$*fiboA1* + *fiboB2*;
  $u_2^*(t)$*weightedMoving*$\leftarrow$*weighted Moving*+ (*ContainerhistoryItem* * *weight*);
  $u_1^*(t)$*_weight*$\leftarrow$*total* $u_0^*(t)$*_weight* + $u_2^*(t)$*weight* $u_3^*(t)$*_weight*;
  i ++;
end while
Min$\{\mathcal{J}(u_1, u_2, u_3)\} \leftarrow$ *Compute Equ* (14)
// Calculate optimality condition $\mathcal{H}$
While $t < T$ ***do***
  Compute *R(t)* and *V(t)* according to (16) and (18) respectively.
  Compute *R(t)*and *V(t)* according to algorithm (1).
  Update queries *R(t)* and *V(t)* according to (5) and (8).
  T $\leftarrow t + 1$
$\mathcal{H}$*_Value*$\leftarrow$ enforce (Equ. 12)
  Pontryagin's maximum principle $\leftarrow$J2 * (*initialValue* - *pastInitialValue*)+ ((1–J2) * *pastTrendPosteriorValue*);
Min$\{\mathcal{J}(u_1, u_2, u_3)\} \leftarrow$*initialValue*+ *trendPosteriorValue*;
Return
End while

5. Illustrative proof of concept

5.1. Post pandemic-X RoboFTOCM with optimal control strategy

This section presents a use case for future transmission dynamics in RoboFTOCM, focusing on an optimal control policy outlined in Algorithm I. The PMP is the backbone of the RoboFTOCM control testbed, and it is fully optimised with carefully chosen parameters. Figure 5 targets rapid infection spread within populations and acts as a rapid intervention tool under the optimal control framework. Considering our earlier work (Okafor et al., 2025), Figure 6 depicts the real-world deployment in a hospital facility. Since the Accident and Emergency (A &E) unit handles more complex tasks such as such as patient monitoring, navigation through busy environments, and interaction with medical staff, this leads to higher CPU and memory utilisation. Consequently, Algorithm I, combined with the power management routine, is employed to complete tasks and enhance computational efficiency. A key challenge addressed is the optimal management of resources despite stochastic job inflows, temporal variability, and imperfect resource estimation. Our algorithm successfully overcomes these dynamic workload challenges without overloading or draining power quickly as illustrated in Figure 7. Equipped with optimal control capabilities (CC) for sensing and intervention, the robot aims to slow the natural transmission of Pandemic-X infections, especially variants of concern (VoC). The system relies on software-defined network (SDN)

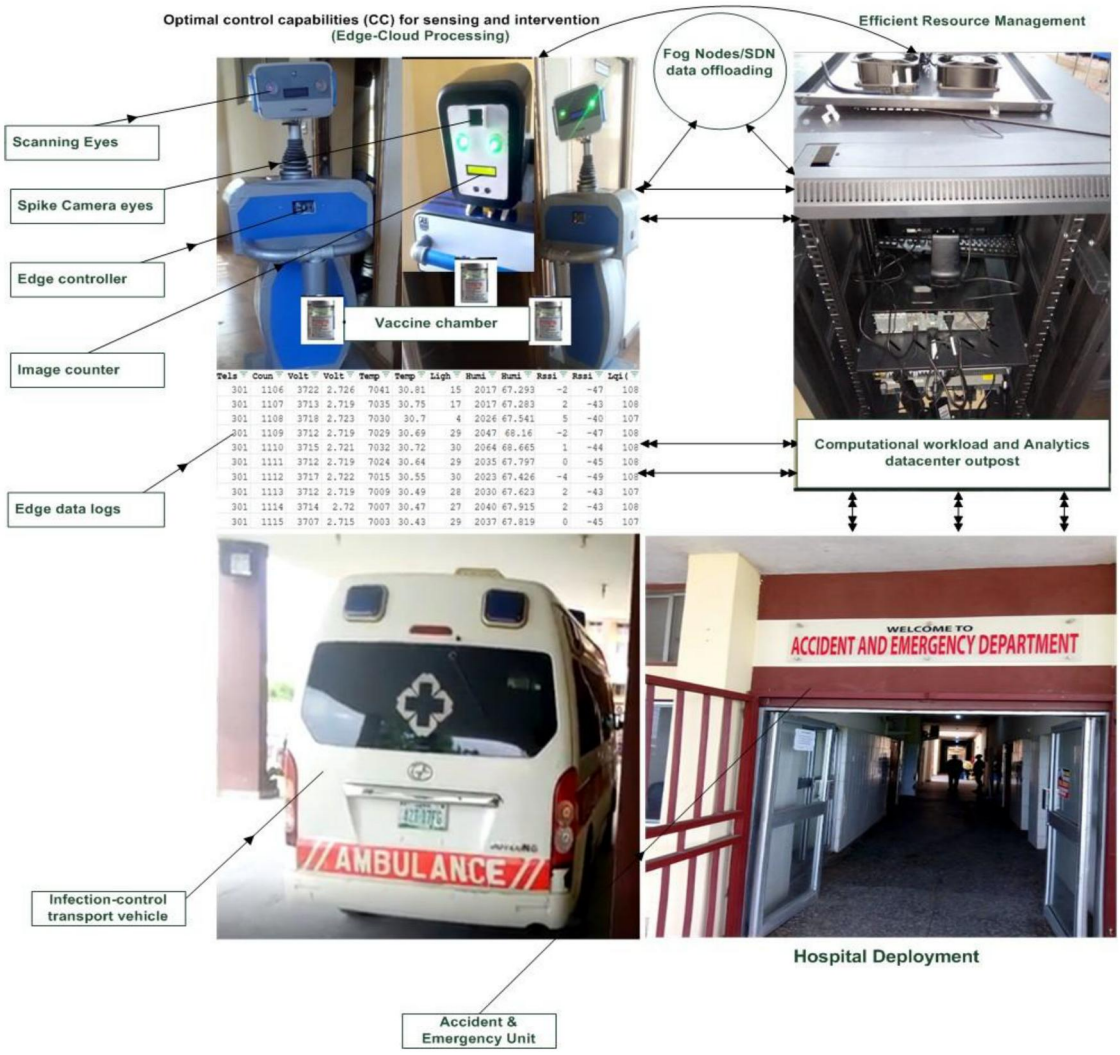

Figure 5. Edge-Enabled Smart Healthcare Robot in A&E. It shows a smart healthcare robot deployed in the A&E unit, performing tasks such as patient monitoring, autonomous navigation, and staff interaction. Edge-based control and a power-aware resource management routine optimise CPU and memory under dynamic workloads, while software-defined networking (SDN) enables low-latency data flow to support real-time sensing, operational efficiency, and infection-mitigation strategies.

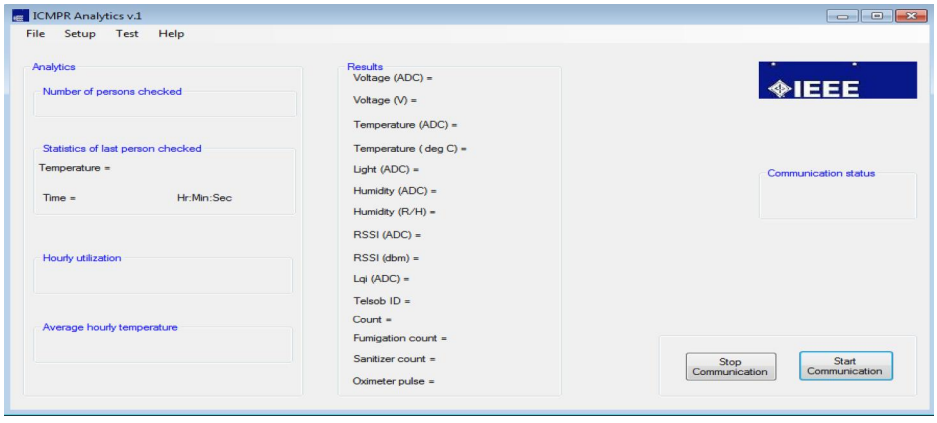

Figure 6. RoboFTOCM Application control testbed dashboard.

datastream flow engine. This incorporates the control capabilities from Algorithm I. To link to the cloud, we used the Fog infrastructure to offload data streams to the cloud via multiplexed multipath routing. During edge deployment, the robot operates with an AI-driven face identification engine integrated

with a temperature screening function alongside other parameters in Table 3. It measures skin surface temperature, reporting anomalies to the private outpost NOC. The spike camera, with 120x160 resolution at 25 frames per second, enables rapid temperature measurement without requiring identity verification. Additionally, the robot features a vaccine injection valve for non-invasive vaccination, an essential element of the strategy illustrated in Figure 5 that significantly impacts its practical deployment.

Figure 6 shows the analytics dashboard of the RoboFTOCM control testbed. This dashboard is used to monitor efforts to mitigate the spread of Pandemic-X infection in the post-Pandemic-X era. It features dynamic control functions based on Pontryagin stochastic optimisation. The start and stop communication keys track the number of people sampled and generate temperature profiles. Hourly readings including oximeter pulse rates, sanitiser usage counts, fumigation status, and signal indicators, are recorded and stored in a historical log file.

5.2. Pandemic-X RoboFTOCM state dynamics and power profiles

Figure 7 illustrates the RoboFTOCM energy conservation strategy at the hospital facility. This scheme makes use of three distinct operational states with each tied to specific workload and computational demands. As a result, it optimised the battery usage and extended operational lifespan at the deployment. For simplicity, we denote these state-codes with Node 301, 302, and 303, which are briefly explained below.

- Node 303—Super-active Mode (Active Edge Inferencing) handles high-computation workloads, especially during active edge inferencing for robotic control, neural processor decision-making, and real-time AI analytics. It corresponds to intensive tasks such as face-mask identification via Spike camera (f) or non-face-mask identification (e), as well as active vaccination states in both Power ON with active vaccination (c) and vertical deployment with mobility support (d). Its mean power consumption is 0.9791 W, the highest among the three modes, reflecting the energy demands of sustained neural computation.
- Node 301—Moderate Mode (Fallback State) operates at a 50% duty cycle, managing essential tasks with reduced processor computation and network activity, serving as a load-balanced fallback when Node 303 is not fully engaged. It supports edge-based network operating centre operations (a) and maintenance states in between intensive inference cycles. Its mean power consumption is 0.4982 W, representing a balance between responsiveness and energy efficiency.
- Node 302—Sleep Mode (Dynamic Idle State) enters a low-power state until an external trigger, such as a sensor event, network call, or operator command, is received, thereby minimising battery drain during idle periods. It is aligned with the power-off state without active vaccination (b) and dismembered units for travel redeployments and recruitments (g). Its mean power consumption is 0.0542 W, providing the greatest energy savings when the system is inactive.

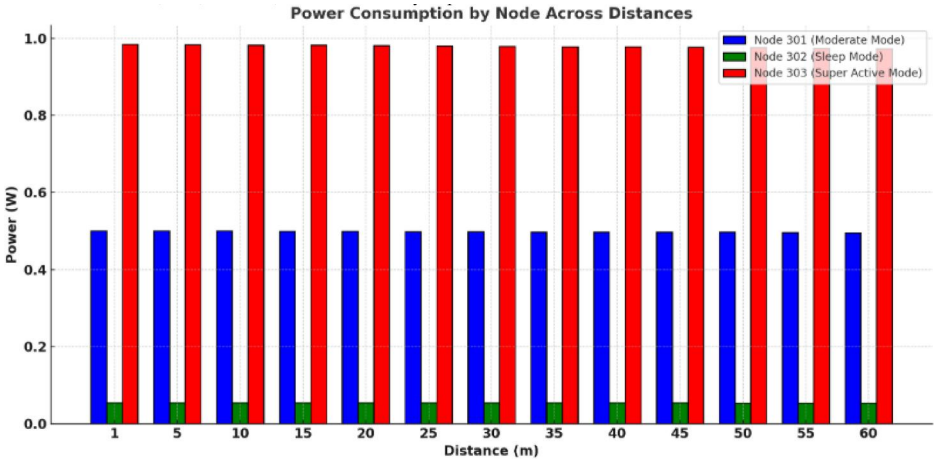

Figure 7. RoboFTOCM energy conservation modes at A & E.

5.3. Energy consumption behaviour

At the edge where RoboFTOCM is deployed, the energy consumption insights show that the mean total system power is 1.5315 W across all states in operation. The total energy usage of over 26 minutes amounts to 0.6636 Wh (calculated as $1.5315\,W \times 26/60\,h$). The combination of dynamic transitions between Node 303 (super-active), Node 301 (moderate), and Node 302 (sleep) ensures that energy-intensive operations are kept time-bound, while low-power states dominate idle and standby phases.

5.4. Operational advantage in smart health infrastructure scenario

The high-intensity states (Node 303) are triggered only during mission-critical phases such as active vaccination (c, d) and AI-based identification (e, f), while moderate states (Node 301) sustain operational readiness, ensuring fast ramp-up when required while halving computational load, and sleep states (Node 302) maintain near-zero consumption until redeployment or triggering events occur (b, g). This tiered state design achieves longer battery life, minimizes heat generation, and reduces overall wear on the battery system, making the deployment more sustainable in mobile, redeployable, and high-uptime environments.

5.5. Shape correlation analytics

We conducted Pearson, Kendall, and Spearman rank correlation analyses to evaluate the significance of RoboFTOCM ambient variables under the control policies in Figure 5. This policy refers to the algorithm that determines how the RoboFTOCM system functions once deployed. We have summarised basic variables in Table 3 with results showing strong internal consistency, with linear mappings between variables. This shows why sensor interdependencies are important. Our correlation analysis reveals valuable insights into sensor calibration, fault detection, and adaptive control strategies. Across all three measures (Pearson, Spearman, and Kendall), the relationship between Voltage (ADC) and Voltage (V) is nearly perfect (0.99998), confirming that these parameters can be interchangeably used in voltage-related control logic with negligible loss of accuracy. A strong positive correlation (0.91247) between Voltage (ADC) and Light (ADC) indicates that lighting variations closely track voltage readings. This is likely due to shared power lines, sensor circuitry, and environmental factors.

Conversely, Voltage (ADC) and Humidity (ADC) show a strong negative correlation in Pearson (−0.91143) and Spearman (−0.90610) measures, while Kendall's Tau suggests a moderate negative relationship (−0.47674). This indicates that as voltage increases, humidity readings tend to decrease possibly due to the humidity sensor's sensitivity to temperature-driven changes affecting power supply or environmental conditions. This relationship can be used for cross-sensor validation, detecting sensor drift or

Table 3. RoboFTOCM test signal parameters.

Parameter pair	Description	Relationship/remarks
Voltage (ADC) and Voltage (V)	• Raw digital value from the analogue-to-digital converter (ADC) reading the voltage sensor. • Actual voltage in volts, obtained by calibrating and scaling the ADC value.	Voltage (ADC) is the unprocessed sensor output; Voltage (V) is the corresponding real-world measurement.
Voltage (ADC) and Light (ADC)	• Voltage (ADC): Raw reading from the voltage sensor. • Light (ADC): Raw reading from the light sensor via ADC	A strong correlation suggests voltage changes are linked to light level variations, possibly due to shared circuits or environmental conditions.
Voltage (ADC) and Humidity (ADC)	• Both are unprocessed ADC readings, one from the voltage sensor and the other from the humidity sensor.	There's a strong negative correlation—higher voltage readings generally coincide with lower humidity readings, likely due to environmental influences.
Received Signal Strength Indicator (RSSI)–ADC	Raw ADC value representing radio signal strength before scaling or calibration.	A unitless digital value used as the initial measure of signal power.
Received Signal Strength Indicator (RSSI)–dBm	Calibrated signal strength, expressed in decibels relative to one milliwatt (dBm).	A standardised measure derived from RSSI (ADC) that allows meaningful comparison across devices.
RSSI (ADC) vs. RSSI (dBm)	RSSI (ADC) is the raw reading; RSSI (dBm) is the calibrated, real-world equivalent.	Both describe the same signal strength, but at different processing stages.

environmental anomalies when deviations from expected patterns occur. Finally, the RSSI (ADC) and RSSI (dBm) readings exhibit a perfect correlation (1.00000) across all metrics, confirming they represent the same measurement on different scales. This flexibility allows either reading to be used reliably for signal strength monitoring without data loss. In practice, these correlation insights support RoboFTOCM firmware optimisation. The goal is to improve sensor sensitivity, and integration, reduce redundant logging, and develop resilient control algorithms that consider multi-sensor dependencies as illustrated in Figure 5.

6. Numerical simulation

In this section, we carried RoboFTOCM simulation based on system model (13). We used real world parameters from StreamRobot (Okafor et al., 2025; Frank et al., 2022), Tuberculosis and Hepatitis B co-infection (Jennings & Ordóñez, 2013), Runge Kutta Optimizer (Mahapatra & Triambak, 2022), Infection Model (Naceri et al., 2022), Fractional-Order Compartmental Model (Mengcan et al., 2021) (See Table 4). The system model in (24) has been earlier described in Section 3 and implemented in MATLAB R2019 (9.6.0.1072779). Also, the effect of various control strategies on the transmission dynamics were explored using parameters in Table 4. This was done by simulating the vaccination (DV) and the control parameters considering the model system (24) over the time interval [0, 100]. The proposed model system (13) is then simulated using the baseline original scenario setup: $S(0) = 5000, V(0) = 1500, E(0) = 2003, A(0) = 416, I(0) = 208, H(0) = 404, T(0) = 115$ and $R(0) = 500$ (Iacoviello & Stasio, 2013; Jafarimoghaddam & Soler, 2023). The optimized parameter values used for the simulation case study are given in Table 3. The step size used for the simulation is $h = 0.02$ *and* $Nh = 100$. The numerical scheme used is based on the Runge-Kutta Method of Order Four (RK-4) (Jennings & Ordóñez, 2013). Table 4 shows the optimal parametric values for the numerical simulation of the disease control strategy.

7. Results & discussions

7.1. Performance analysis

This section compares the performance of the proposed optimal control scheme with a non-optimal case study. First, we generated all parametric inputs using Table 4. The three interventions were then simultaneously implemented and simulated using the optimal models (1a) and (11). Considering the optimal control of Pandemic-X with robotic identification model system (1a), we solved the optimality system and numerically simulated the optimal system (11) by considering the three controls (i.e. vaccination u_1, robotic identification u_2 and treatment u_3). The results are then presented in Figures 8–12. The effect of vaccination, robotic identification, and treatment on the susceptible, exposed, asymptomatically infected, symptomatically infected, and treated/recovered individuals is observed. It has been seen that optimal control measures significantly influence the susceptible, exposed, asymptomatically infected, symptomatically infected, and treated/recovered individuals.

Figure 8, (blue and red curve) respectively illustrates that when the vaccination rate among the susceptible population is low $(u_1 = 0.0000075, or\ 0.00075)$, robotic detection $(u_2 = 0.000090771\ or$

Table 4. Numerical simulation parameters.

Parameters	Value	Source	Parameters	Value	Source
φ	750	(Naceri et al., 2022)	υ	$0-1$	Optimised
η	$0-1$	(Bowong & Kurths, 2010)	σ	$0-1$	Optimised
ω	$0-1$	(Bowong & Kurths, 2010)	γ	$0-1$	Optimised
ϖ	0.0007	(Bowong & Kurths, 2010)	κ	0.00286	(Okafor & Longe, 2022)
β	0.0000124	(Okafor & Longe, 2022)	Δ	0.00286	(Okafor & Longe, 2022)
α_1	$00.02-2$	(Bowong & Kurths, 2010)	ξ	0.1109289	(Okafor & Longe, 2022)
ρ	0.2516	Optimised	θ	0.0022927	(Okafor & Longe, 2022)
α_2	$0.02-2$	(Bowong & Kurths, 2010)	ψ	0.4	(Krishn & Prakash, 2020)
μ	0.003324588	(Okafor & Longe, 2022)	δ	0.2	(Krishn & Prakash, 2020)
τ	$0.01-0.3$	Optimised	Λ	0.02	Optimised
ϱ	0.25001	Optimised	π	60	(Frank et al., 2022)
$\emptyset$	0.000011618	(Okafor & Longe, 2022)	$\hat{\pi}$	30	Optimised
ε	0.0668	(Yousri et al., 2022)	t	100	Optimised

0.0090771), and treatment of the Isolated/Hospitalized ($u_3 = 0.0000001109289$ *or* 0.00001109289), are ineffective, individuals exposed to Pandemic-X are at a higher risk of contracting and spreading the virus. This situation increases the number of exposed cases and the potential for new variants to emerge. Moreover, those who are unvaccinated or lack access to robotic detection may face more severe symptoms and complications, which can strain the healthcare system, leading to more hospitalizations and deaths. Conversely, Figure 8 (green curve) also shows that increasing the vaccination rate ($u_1 = 0.75$) among the susceptible population, along with effective robotic detection ($u_2 = 0.90771$) and effective treatment of the Isolated/Hospitalized ($u_3 = 0.1109289$), significantly reduces the likelihood of exposed individuals becoming infected or experiencing severe symptoms. This combination limits the virus's spread by decreasing the number of exposed individuals. Additionally, a high vaccination rate coupled with effective robotic detection lowers the chances of new variants emerging, as there are fewer opportunities for the virus to mutate. Over time, this can reduce the overall threat of Pandemic-X infection.

Figures 9 and 10, (blue and red curves respectively) show that in scenarios with low vaccination rates ($u_1 = 0.00075, or\ 0.075$) among the susceptible population, ineffective robotic detection ($u_2 =$ 0.0090771 *or* 0.090771) and ineffective treatment of the Isolated/Hospitalized ($u_3 = 0.00001109289$ *or* 0.001109289), the number of asymptomatically and symptomatically infected individuals increases. Consequently, these individuals are more likely to spread the infection, potentially causing a surge in cases. This situation poses a significant risk to unvaccinated individuals. However, the green curve shows that an increased vaccination rate ($u_1 = 0.75$) among the susceptible population with effective robotic detection control ($u_2 = 0.90771$) and effective treatment of the Isolated/Hospitalized ($u_3 = 0.1109289$) leads to a decrease in both asymptomatically and symptomatically infected individuals (as depicted in Figures 9 and 10, respectively). Specifically, the asymptomatically and symptomatically infected curves shows a gradual rise, indicating a higher transmission rate (blue and red respectively), due to ineffective control and increased contact rates. In contrast, the green exhibits a steeper decrease in the asymptomatically and symptomatically infected, especially in the early phase, suggesting a faster and more aggressive control of the disease. These differences in infection velocity highlight the impact of control

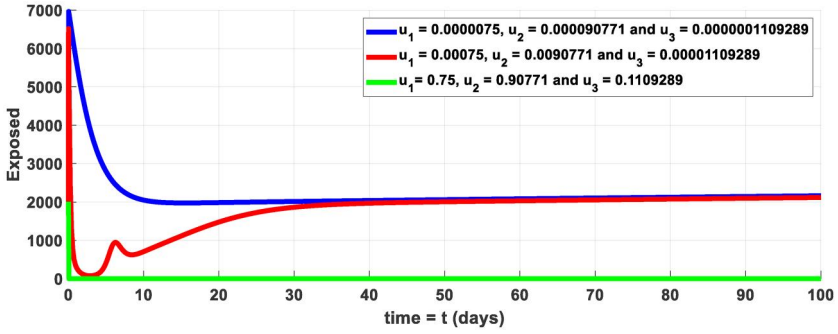

Figure 8. Dynamics of exposed individuals when different combination of optimal controls strategies is applied at a time. $(i.e., 0 \leq u_1, u_2, u_3 \leq 1)$

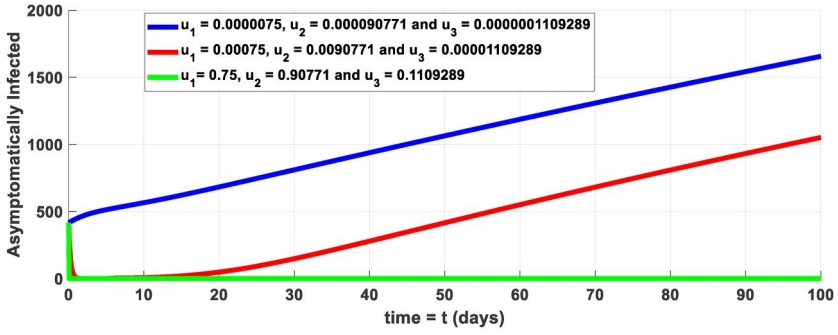

Figure 9. Dynamics of asymptomatically infected individuals when different combination of optimal control strategies is applied at a time $(i.e., 0 \leq u_1, u_2, u_3 \leq 1)$.

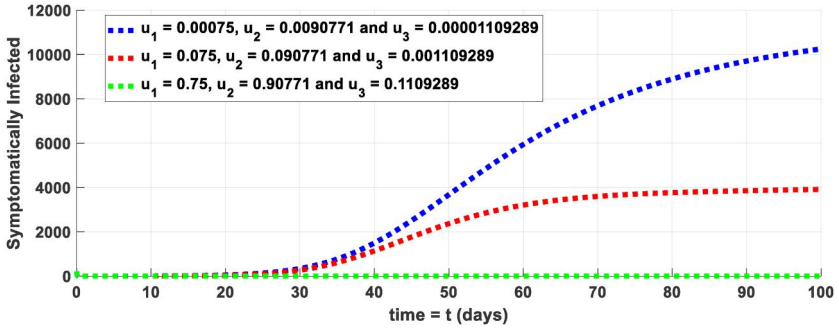

Figure 10. Dynamics of symptomatically infected individuals when different combination of optimal control strategies is applied at a time. $(i.e., 0 \leq u_1, u_2, u_3 \leq 1)$

Table 5. Distribution of the number of exposed, asymptomatically and symptomatically infected using the control scenarios.

Control parameters	Low	Moderate	High
u_1	$7.5E^{-6}$	$7.5E^{-4}$	$7.5E^{-1}$
u_2	$9.0771E^{-4}$	$9.0771E^{-3}$	$9.0771E^{-1}$
u_3	$1.109289E^{-7}$	$1.109289E^{-5}$	$1.109289E^{-1}$
Number of exposed in 100 days	2162.42	2117.48	$6.9409E^{-6}$
Number of asymptomatically infected in 100 days	1656.33	1051.03	$4.80E^{-5}$
Number of asymptomatically infected in 100 days	10249.78	3913.70	$4.80E^{-25}$

strategies on Pandemic X: increased rates reflect weaker interventions, while decreased rates suggest timely and effective containment measures. The distinction across the scenarios is crucial in assessing the urgency and type of intervention required to mitigate the Pandemic X outbreak effectively. This decrease results in a lower likelihood of virus transmission due to better treatment control, reducing the overall infection transmission rate in the population (i.e., asymptomatically, and symptomatically infected individuals).

Figures 8–10 demonstrate the effectiveness of increasing the intensity of control strategies—vaccination (u_1), effective detection (u_2), and treatment (u_3)—in reducing disease spread over a 100-day simulation period. Under low control levels, the number of exposed individuals remains high at 2162.42, while the asymptomatic and symptomatic infections reach 1656.33 and 10249.78 respectively, indicating a significant burden of hidden and active Pandemic X infections. As control levels move from low to moderate, all three compartments show noticeable reductions. Specifically, the exposed population drops slightly to 2117.48, the asymptomatic infections decrease more substantially to 1051.03, and the symptomatic cases reduce to 3913.70. This suggests that even a moderate increase in control efforts particularly through detection and treatment yields meaningful containment of the epidemic.

Under high control levels, the impact is dramatic. The number of exposed individuals falls to approximately 6.94×10^{-6}, effectively reaching zero. Similarly, asymptomatic and symptomatic infections plummet to 4.80×10^{-5} and 4.80×10^{-25} respectively, indicating near-complete suppression of disease transmission. These results affirm that the combined high implementation of vaccination, proactive detection, and treatment leads to eradication of the disease within the population in the simulation window. This is also evident in Table 5, which highlights that while moderate control can mitigate the spread, it is the high-level implementation of all three interventions simultaneously that achieves optimal epidemic control emphasising the need for integrated and aggressive public health responses during outbreaks.

Figure 11 illustrates the dynamics of isolated/hospitalised individuals when different combinations of optimal control strategies are applied simultaneously. $(i.e., 0 \leq u_1, u_2, u_3 \leq 1)$. It's observed that with different optimal control strategies, such as low vaccination rates among the susceptible population and ineffective robotic detection, hospitals become overburdened. This happens because when fewer people are vaccinated, the virus spreads more easily, leading to an increase in cases. Additionally, ineffective robotic detection can cause delays in response, further exacerbating the virus's spread. Conversely, a high vaccination rate among the susceptible population with effective robotic detection control

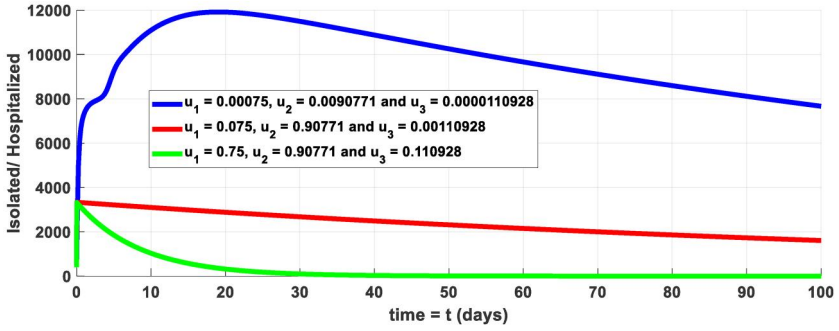

Figure 11. Dynamics of isolated/hospitalised individuals when different combination of optimal control strategies is applied at a time. $(i.e., 0 \leq u_1, u_2, u_3 \leq 1)$

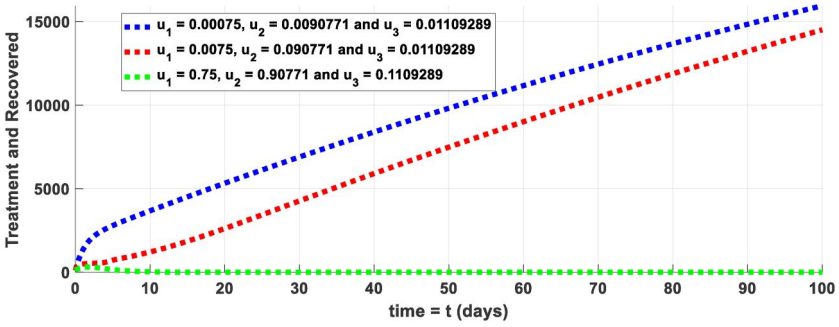

Figure 12. Dynamics of treated/recovered individuals when different combination of optimal control strategies are applied at a time. $(i.e., 0 \leq u_1, u_2, u_3 \leq 1)$

significantly reduces the number of severely infected individuals, thereby decreasing the number of isolated/hospitalised individuals.

In Figure 12, the dynamics of treated/recovered individuals under various optimal control strategies $(i.e., 0 \leq u_1, u_2, u_3 \leq 1)$ are illustrated. It's evident that a low vaccination rate among the susceptible population with ineffective robotic detection can overwhelm treatment facilities. This scenario results in more people being susceptible to the infection, leading to higher case numbers and hospitalisations, burdening the treatment facilities due to the high number of individuals needing treatment. Conversely, an increase in the vaccination rate among the susceptible population with effective robotic detection decreases the number of treated/recovered individuals since fewer people get infected, as shown in Figure 12. This decrease is due to the high vaccination rate reducing the overall infection numbers, making it easier to provide adequate treatment to those infected. Effective robotic detection allowed for the rapid identification and isolation of infected individuals, reducing the chances of further infection spread. Consequently, the population treated for Pandemic-X infection has a better chance of recovery, reducing the overall burden on the healthcare system due to a significant decrease in the population of treated/recovered individuals. However, the number of exposed, asymptomatic, and symptomatically infected individuals is minimised due to the effect of the optimal control strategies outlined in this paper.

Figures 11 and 12 show the distribution of hospitalised and isolated/treated individuals over 100 days under low, moderate, and high levels of vaccination (u_1), detection (u_2), and treatment (u_3). As seen in Table 6, low control results in 7665.96 hospitalisations and 15885.26 isolated/treated cases, indicating a heavy strain on healthcare. Moderate control reduces hospitalisations to 1609.45 and slightly lowers isolation/treated numbers to 14497.74, suggesting some improvement. Under high control, both indicators drop drastically—hospitalisations to 2.7419×10^{-2} and isolation to 1.5803×10^{-16}—showing near-total suppression of severe cases. These outcomes highlight the critical role of combined, intensive interventions in reducing Pandemic-X disease burden and relieving healthcare pressure.

Table 6. Distribution of the number of hospitalised and isolated/treated using the control scenarios.

Control parameters	low	moderate	high
u_1	$7.5E^{-4}$	$7.5E^{-2}$	$7.5E^{-1}$
u_2	$9.0771E^{-3}$	$9.0771E^{-1}$	$9.0771E^{-1}$
u_3	$1.109289E^{-5}$	$1.109289E^{-5}$	$1.109289E^{-1}$
Number of Hospitalized in 100 days	7665.96	1609.45	$2.7419E^{-2}$
Number of Isolated/Treated in 100 days	15885.26	14497.74	$1.5803E^{-16}$

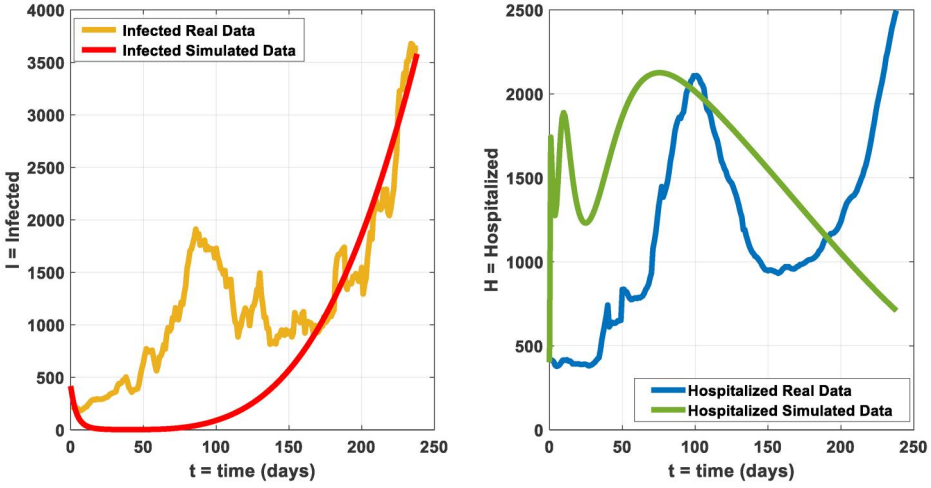

Figure 13. Computational comparison between real and simulated data in the absence of vaccination.

7.2. Model fitting and validations

This subsection describes a validation study using real-world datasets. Data for hospitalisation, vaccination cases of Pandemic-X infection were collected from Johns Hopkins University and Medicine. To validate the computational model, both real and simulated data were utilised. The real data were fitted to the model described in Equation (1a). These data were gathered daily from 21st April to 14th December 2020 and from 15th December 2020 to 11th April 2021 (Johns Hopkins University & Medicine, 2024) representing the number of individuals who were hospitalised, vaccinated or tested positive for Pandemic-X during this specified timeframe. The model's results were then fitted using the parameters outlined in Table 4.

We further conducted a comparison between real and simulated Pandemic-X data to highlight the impact of vaccination and robotic control on pandemic outcomes. Both data sets show a rise in vaccinations, reflecting increased availability and uptake, and achieve comparable vaccination levels by 118 days, indicating effective coverage. Infection rates decrease in both scenarios due to increased vaccinations, leading to slower virus spread. Initial increases in hospitalisations match rising infections, but the simulated model with robotic control stabilises hospitalisations more quickly. Both datasets converge after day 70, suggesting effective management of severe cases and similar overall outcomes. This work encapsulates how vaccination and robotic control influence the dynamics of Pandemic-X in both real and simulated environments. Throughout the rest of this paper, infectious disease models shall be referred to as Pandemic-X. Results show that as vaccination campaigns progress, real and simulated data reveal an increasing vaccination rate with a decreasing infected population. These findings highlight the importance of combining vaccination with CIoT and robotic control for effective pandemic management in the post-pandemic era.

Figure 13 presents a computational comparison between real-world and simulated data for Pandemic-X, specifically under a control scenario involving robotic detection (u_2) of infected individuals without the inclusion of vaccination (u_1). The simulation highlights the effect of early identification and isolation of asymptomatic and symptomatic individuals on infection and hospitalisation trends over 250 days. In the left panel, the real infection data (gold line) displays a highly volatile pattern with multiple peaks, characteristic of delayed response, behavioural variability, and external shocks such as variant emergence or policy shifts. In contrast, the simulated infection curve (red line) initially drops due to the immediate effect of robotic detection but begins to rise significantly around day 100. This

exponential growth—although smoother—suggests that detection alone, without vaccination, is insufficient to suppress transmission, especially in the face of increased community spread and latent carriers who may escape detection thresholds. The right panel offers a more revealing perspective on the impact of robotic detection on healthcare burden. The simulated hospitalisation curve (green line) remains notably lower and more stable than the real hospitalisation data (blue line), which exhibits sharp fluctuations and periodic surges. The ability of robotic detection to lower hospital admissions over time reflects its success in identifying and isolating cases early, thereby preventing progression to severe illness and reducing stress on healthcare infrastructure.

However, the continued rise in infections in the absence of vaccination highlights a key limitation: robotic detection alone cannot halt transmission chains, especially when immunity gaps remain unaddressed. The model underscores the need for a multi-pronged approach, where robotic detection is used in tandem with vaccination to achieve both containment and suppression.

Consequently, the simulation confirms that robotic detection contributes significantly to reducing hospitalisation and managing clinical load, but its influence on infection rates is temporary and non-sustainable without immunological interventions. These findings reinforce the importance of integrated control strategies—combining technological tools with biological interventions—for long-term epidemic management.

Figure 14 illustrates the observed patterns in real and simulated COVID-19 data, highlighting vaccination effects in both and robotic control in the simulation. A brief explanation is provided below.

The application of optimal control strategies—vaccination (u_1), detection of asymptomatic infections (u_2), and treatment of symptomatic individuals (u_3)—aims to mitigate both the spread and impact of Pandemic-X. A comparative analysis of real and simulated data provides critical insights into the time-dependent effectiveness of these interventions. As observed in Figure 14, there is an initial similarity between the real and simulated trajectories of infected individuals, particularly during the early phase of the epidemic (days 0–40). This initial alignment highlights the delay in the observable impact of control strategies, a phenomenon commonly seen in real-world settings where interventions such as vaccination and mass testing require time to reach effective thresholds across the population. However, from approximately day 40 onwards, the simulated infection curves begin to diverge significantly from the real data, demonstrating a gradual and sustained decline that reflects the compounded effect of optimal interventions. The simulated vaccination curve exhibits a more consistent and steadily increasing trend than the real-world vaccination data, indicating the benefit of a coordinated and timely rollout strategy. Furthermore, the hospitalisation data provides strong evidence of the model's ability to alleviate pressure on the healthcare system. The simulated values show a marked reduction in hospital admissions compared to the real data, especially after the first few weeks, underscoring the role of early intervention in preventing healthcare system overload. This temporal pattern supports the notion that optimal control strategies do not yield instantaneous results but rather operate through delayed but sustained

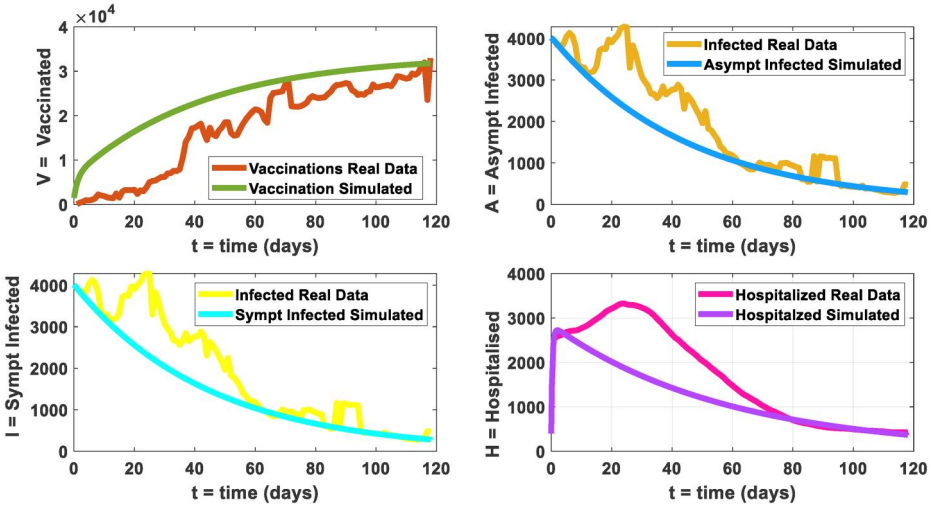

Figure 14. Computational comparison between real and simulated data in the presence of vaccination.

effects, especially in the presence of complex human behaviours, logistical constraints, and transmission dynamics. Consequently, while the model may not eliminate early surges in infection, it effectively flattens the curve, reduces peak burdens, and shortens the epidemic tail—outcomes that are central to public health resilience. Summarily, the findings highlight the critical importance of timely, sustained, and adaptive implementation of control measures. They also reinforce the utility of mathematical modelling in designing realistic, data-informed strategies that balance immediate response with long-term epidemic management.

7.3. Current limitations

Despite the strengths of the optimal model system, some challenges remain when deploying infrastructure robots (Cot) in real-world environments such as hospitals and healthcare facilities. Two main limitations are observed:

- The robotic system sometimes struggles to reliably identify certain elderly individuals and people with disabilities, even though combined features like face mask detection, voice, and tactile inputs help mitigate this issue.
- Navigating crowded areas and smaller spaces not designed for wheeled robots can be difficult, which poses challenges for concurrent vaccination efforts.

8. Conclusion

This paper presented *RoboFTOCM* as an optimal control strategy to manage future pandemic transmission dynamics, using Pontryagin's maximum principle. Our results demonstrate that combining high vaccination rates with robotic interventions significantly reduces the number of susceptible, exposed, asymptomatic, symptomatic, isolated/hospitalised, and recovered individuals. Increasing vaccination lowers susceptibility and transmission, while robotic control improves contact tracing and isolation, further curbing infections. The study quantitatively showed that optimal vaccination alongside robotic identification and treatment effectively reduces exposed and infected cases across different stages. Incorporating a saturated incidence rate model realistic transmission limits, robotic control reduces human exposure, and vaccination increases population immunity; together, these strategies substantially diminish Pandemic-X incidence. Future work will focus on training robots for lightweight resource management, exploring computational transformations based on DNA cloning, and analysing cost and weight functions with real-world data. We also plan to integrate advanced AI techniques, develop co-infection and multi-disease models, and design adaptive vaccination protocols that respond to immunity waning and pathogen mutations. Empirical validation with diverse datasets will further enhance model reliability and applicability.

Acknowledgments

We extend our sincere gratitude to the Ethics Committee of the University of Calabar Teaching Hospital (UCTH) for their invaluable support and guidance in facilitating the COVID-19 Marketplace Robot project. Our special thanks go to Dr. Iheanacho, Obinna Ebere, whose speciality expertise and dedication were instrumental in the successful implementation of this initiative.

Author contributions

CRediT: **Kennedy Chinedu Okafor**: Conceptualization, Data curation, Formal analysis, Funding acquisition, Investigation, Methodology, Resources, Software, Supervision, Validation, Visualization, Writing – original draft; **Omowunmi Mary Longe**: Data curation, Formal analysis, Supervision, Visualization, Writing – review & editing; **Kelvin Anoh**: Conceptualization, Data curation, Investigation; **Ijeoma Peace Okafor**: Formal analysis, Investigation, Resources, Validation; **Titus Ifeanyi Chinebu**: Conceptualization, Data curation, Formal analysis, Investigation, Software, Validation, Visualization, Writing – review & editing; **Ikechukwu Ignatius Ayogu**: Data curation, Formal analysis, Investigation, Methodology.

Credit authorship contribution statement

All the authors have read and approved the final version of the manuscript.

Kennedy Chinedu Okafor: Writing–review & editing, Conceptualisation, Formal analysis, Validation, Methodology, Funding acquisition. **Titus Ifeanyi Chinebu:** Writing–original draft, Conceptualisation, Writing–review & editing. **Omowunmi Mary Longe, Omowunmi Mary Longe**, Writing–review & editing. **Okafor Ijeoma Peace**: Writing–review & editing. **Kelvin Anoh, Omowunmi Mary Longe**: Writing–review, editing, supervision. **Ikechukwu Ignatius Ayogu**: Writing–review & editing.

Disclosure statement

No potential conflict of interest was reported by the authors.

Ethics statement

This study strictly adhered to the ethical principles and guidelines of the Ethics Committee of the University of Calabar Teaching Hospital (UCTH), with ethics approval number UCTH/CS&T/156/82. No human participants were involved, as the study employed a purely analytic approach. Additionally, permissions were obtained from Johns Hopkins University to use the dataset.

Funding

This research is an extended work on 'IEEE COVID-19 MARKETPLACE Robot' funded by IEEE, USA, and partly sponsored by the Nigeria Tertiary Education Fund under the grant number TETF/ES/UNIV/IMO STATE/TSAS/2021.

About the authors

Professor Kennedy Chinedu Okafor holds a PhD in Digital Electronics and Computer Engineering from the University of Nigeria, Nsukka, and completed postdoctoral research in Mechatronics & Software Engineering at Manchester Metropolitan University and Imperial College London, UK. He is a visiting researcher at the University of Chichester, UK, a senior researcher at the Department of Electrical and Electronic Engineering Science, University of Johannesburg, and teaches and supervises PhDs and postdocs at the Federal University of Allied Health Sciences, Nigeria. His research spans AI and cloud engineering, cyber-physical systems, networked robotics, and digital infrastructure optimisation. He is also Director of the IEEE SkillUp Hub, Region 8, UK.

Professor Omowunmi Mary Longe holds a PhD in Electrical and Electronic Engineering from the University of Johannesburg, South Africa, and is Chair of the Smart Power and Energy Research Group. Her expertise includes electromobility, renewable energy technologies, microgrid design, distributed generation and storage, smart energy systems, and gender issues in energy access.

Dr Kelvin Anoh holds a PhD in Communication Engineering from the University of Bradford, UK, and an MSc in Data Telecommunications and Networks from the University of Salford, UK. He is Director of the Centre for Future Technologies and Senior Lecturer at the University of Chichester, UK, and has served as a Visiting Associate Professor at Novena University, Nigeria, since 2015. His research focuses on smart social infrastructure, AI, signal processing, and interdisciplinary engineering.

Dr Ijeoma Peace Okafor holds a Bachelor of Medicine from the University of Port Harcourt, Nigeria, and an MSc from Cardiff Metropolitan University, UK. As a Senior Specialty Doctor, she contributes to interdisciplinary research bridging engineering and public health sciences, with a focus on the social dimensions of technology adoption, digital health, and population health systems.

Dr Titus Ifeanyi Chinebu holds a PhD in Applied Mathematics from the University of Nigeria, Nsukka, and is a Senior Lecturer at the Federal University of Allied Health Sciences, Enugu. His research focuses on mathematical and computational modelling, computational biomedical systems, and interdisciplinary applications in health infrastructure.

Dr Ikechukwu Ignatius Ayogu holds a PhD and is a Lecturer in the Department of Computer Science at the Federal University of Technology, Owerri, Nigeria. His research spans Artificial intelligence, machine learning, natural language processing, cybersecurity, and computational systems for digital infrastructure.

ORCID

Kennedy Chinedu Okafor http://orcid.org/0000-0002-9243-6789

Data availability statement

Data related to those figures/tables will be made available upon reasonable request from the corresponding author.

References

Afful, B. A., Safo, G. A., Marri, D., Okyere, E., Ohemeng, M. O., & Kessie, J. A. (2025). Deterministic optimal control compartmental model for COVID-19 infection. *Modeling Earth Systems and Environment*, *11*(2), 87. https://doi.org/10.1007/s40808-024-02183-0

Athawale, T. M., Johnson, C. R., Sane, S., & Pugmire, D. J (2023). Fiber uncertainty visualization for bivariate data with parametric and nonparametric noise models. *IEEE Transactions on Visualization and Computer Graphics*, *29*(1), 613–623. https://doi.org/10.1109/TVCG.2022.3209424]

Bongard, J. (2008). Probabilistic robotics. Sebastian Thrun, Wolfram Burgard, and Dieter Fox. (2005, MIT Press.) 647 pages. *Artificial Life*, *14*(2), 227–229. https://doi.org/10.1162/artl.2008.14.2.227

Bowong, S., & Kurths, J. (2010). Modelling turberculosis and hepatitis B co-infection. *Math. Model. Nat. Phenom*, *5*(6), 196–242.

Cai, Z., Fu, Q., Zhang, S., Guo, S., Guo, J., Zhang, X., & Fan, C. (2022). Characteristic analysis of a magnetically actuated capsule microrobot in medical applications. *IEEE Transactions on Instrumentation and Measurement*, *71*, 1–11. https://doi.org/10.1109/TIM.2021.3130299

Cao, H., Huang, X., Song, Y., & Lewis, F. L. (2024). Cooperative control of multiagent systems: A quantization feedback-based event-triggered approach. *IEEE Trans. on Cybernetics*, *54*(3), 1960-1971. https://doi.org/10.1109/TCYB.2023.3307099

Chen, B., Hu, J., Zhao, Y., & Ghosh, B. K. (2022). Finite-time observer-based tracking control of uncertain heterogeneous underwater vehicles using adaptive sliding mode approach. *Neurocomputing*, *481*, 322–332. https://doi.org/10.1016/j.neucom.2022.01.038

Coronavirus. (2023). (COVID-19) Latest insights: Infections. https://www.ons.gov.uk/peoplepopulationandcommunity/healthandsocialcare/conditionsanddiseases/articles/coronaviruscovid19latestinsights/infections

Di Lallo, A., Murphy, R., Krieger, A., Zhu, J., Taylor, R. H., & Su, H. (2021). Medical robots for infectious diseases: Lessons and challenges from the COVID-19 pandemic. *IEEE Robotics & Automation Magazine*, *28*(1), 18–27. https://doi.org/10.1109/MRA.2020.3045671

Ding, X., Shang, B., Xie, C., Xin, J., & Yu, F. (2025). Artificial intelligence in the COVID-19 pandemic: Balancing benefits and ethical challenges in China's response. 1. *Humanities and Social Sciences Communications*, *12*(1)19. https://doi.org/10.1057/s41599-025-04564-x

Eihab, B. M. B., & Kailash, C. P. (2017). Optimal control of an epidemiological model with multiple time delays. *Applied Mathematics and Computation*, *292*, 47–56. https://doi.org/10.1016/j.amc.2016.07.009

Escosio, R. A. S., Cawiding, O. R., Hernandez, B. S., et al. (2022). A model-based strategy on COVID-19 vaccine roll-out in the Philippines. *medRxiv*. 1-17. https://doi.org/10.1101/2022.05.27.22275675

Fang, Z., Sun, H., & Wang, H. (2020). A fast method for variable-order Caputo fractional derivative with applications to time-fractional diffusion equations. *Computers & Mathematics with Applications*, *80*(5), 1443–1458. https://doi.org/10.1016/j.camwa.2020.07.009

Forrest, O., & Al-Arydah, M. (2025). Optimal control strategies for infectious diseases with consideration of behavioral dynamics. *Mathematical Methods in the Applied Sciences*, *48*(2), 1362–1380. https://doi.org/10.1002/mma.10388

Frank, F., Paraschos, A., van der Smagt, P., & Cseke, B. Aug (2022). Constrained probabilistic movement primitives for robot trajectory adaptation,. *IEEE Transactions on Robotics*, *38*(4), 2276–2294. https://doi.org/10.1109/TRO.2021.3127108

Gui-Quan, S., Hong-Tao, Z., Li-Li, C., Zhen, J., Hao, W., & Shigui, R. (2022). Dynamics of a diffusive foot-and-mouth disease model with nonlocal infections. *SIAM Journal on Applied Mathematics*, *82*(4), 1587–1610.

Guo, Q. (2023). Optimal robust control of electro-hydraulic system based on Hamilton–Jacobi–bellman solution with backstepping iteration. *IEEE Transactions on Control Systems Technology*, *31*(1), 459–466. https://doi.org/10.1109/TCST.2022.3174772

Holst, M., & Licht, M. (2023). Geometric transformation of finite element methods: Theory and applications. *Applied Numerical Mathematics*, *192*, 389–413. https://doi.org/10.1016/j.apnum.2023.07.002

https://commonslibrary.parliament.uk/research-briefings/cbp-9309/

Huang, S., Li, Y., & Wu, J. (2022). Distributed state estimation for linear time-invariant dynamical systems: A review of theories and algorithms. *Chinese Journal of Aeronautics*, *35*(6), 1–17. https://doi.org/10.1016/j.cja.2021.06.010

Iacoviello, D., & Stasio, N. (2013). Optimal control for sirc epidemic outbreak. *Computer Methods and Programs in Biomedicine*, *110*(3), 333–342. https://doi.org/10.1016/j.cmpb.2013.01.006

Jafarimoghaddam, A., & Soler, M. (2023). Time-fuel-optimal navigation of a commercial aircraft in cruise with heading and throttle controls using Pontryagin's maximum principle. *IEEE Control Systems Letters*, *7*, 2970–2975. https://doi.org/10.1109/LCSYS.2023.3288471

Jain, K., Bhattacharjee, A., & Krishnamurhty, S. (2025). Mathematical analysis of COVID-19 and TB co-infection dynamics with optimal control. *Modeling Earth Systems and Environment*, *11*(1), 65. https://doi.org/10.1007/s40808-024-02197-8

Jamshidi, M. B., Lalbakhsh, A., Talla, J., Peroutka, Z., Hadjilooei, F., Lalbakhsh, P., Jamshidi, M., Spada, L. L., Mirmozafari, M., Dehghani, M., Sabet, A., Roshani, S., Roshani, S., Bayat-Makou, N., Mohamadzade, B., Malek, Z., Jamshidi, A., Kiani, S., Hashemi-Dezaki, H., & Mohyuddin, W. (2020). Artificial intelligence and COVID-19: Deep learning approaches for diagnosis and treatment. *IEEE Access: practical Innovations, Open Solutions*, *8*, 109581–109595. https://doi.org/10.1109/ACCESS.2020.3001973

Jennings, A. L., & Ordóñez, R. (2013). Unbounded motion optimization by developmental learning. *IEEE Transactions on Cybernetics*, *43*(4), 1178–1188. https://doi.org/10.1109/TSMCB.2012.2226026

Jiang, J., Zhu, P., Li, H., Guo, Y., Chen, F., & Lin, M. (2022). Prevention and control strategy of COVID-19. *Disaster Medicine and Public Health Preparedness*, *16*(6), 2210–2210. https://doi.org/10.1017/dmp.2021.180

Jiang, Y., Kang, J., Niyato, D., Ge, X., Xiong, Z., Miao, C., & Shen, X. (2023). Reliable distributed computing for metaverse: A hierarchical game-theoretic approach. *IEEE Transactions on Vehicular Technology*, *72*(1), 1084–1100. https://doi.org/10.1109/TVT.2022.3204839

Johns Hopkins University & Medicine. (2024). County testing data from JHU CCI; cases and deaths data from JHU CSSE; demographic data from American Community Survey https://coronavirus.jhu.edu/region/us/alabama

Joshi, A. A., Chatterjee, D., & Banavar, R. N. (2022). Robust discrete-time pontryagin maximum principle on matrix lie groups. *IEEE Transactions on Automatic Control*, *67*(7), 3545–3552. https://doi.org/10.1109/TAC.2021.3100553

Jung, E., Lenhart, S., & Feng, Z. (2002). Optimal control of treatments in a two–strain tuberculosis model. *Discrete and Continuous Dynamical Systems - B*, *2*(4), 473–482. https://doi.org/10.3934/dcdsb.2002.2.473

Kangzhen, Y. (2017). Strengthen early warning and forecast to reduce the risk of epidemic. *China Feed*, *l3*, 3.

Kantner, M., & Koprucki, T. (2020). Beyond just "flattening the curve": Optimal control of epidemics with purely non-pharmaceutical interventions. *Journal of Mathematics in Industry*, *10*, 23. https://doi.org/10.1186/s13362-020-00091-3

Ketcheson, D. I. (2021). Optimal control of an SIR epidemic through finite-time non-pharmaceutical intervention. *Journal of Mathematical Biology*, *83*(1), 7. https://doi.org/10.1007/s00285-021-01628-9

Khan, M., & Tanimoto, J. (2025). A new concept of optimal control for epidemic spreading by vaccination technique for assessing social optimum employing pontryagins maximum principle. https://arxiv.org/abs/2501.07053

Kipka, R., & Gupta, R. (2019). The discrete-time geometric maximum principle. *SIAM Journal on Control and Optimization*, *57*(4), 2939–2961. https://doi.org/10.1137/16M1101489

Kokurin, M. M., Kokurin, M., & Semenova, A. V. (2022). Iteratively regularized Gauss–Newton type methods for approximating quasi–solutions of irregular nonlinear operator equations in Hilbert space with an application to COVID–19 epidemic dynamics. *Applied Mathematics and Computation*, *431*, 127312. https://doi.org/10.1016/j.amc.2022.127312

Krishn, M. V., & Prakash, J. (2020). Mathematical modelling on phase-based transmissibility of corona virus2. *Infect Dis Model*, *5*, 375–385.

Lee, J., Kim, E., Kim, S., Jeon, S., & Choi, H. (2016 A flexible microrobot with magnetic actuation for medical tool [Paper presentation]. 2016 13th Int [Paper presentation]. 'l Conf. on Ubiquitous Robots and Ambient Intel (URAI), Xi'an, China, pp. 184–185. https://doi.org/10.1109/URAI.2016.7625732

Li, D., Yu, H., Tee, K. P., Wu, Y., Ge, S. S., & Lee, T. H. (2022). On time-synchronised stability and control. *IEEE Transactions on Systems, Man, and Cybernetics: Systems*, *52*(4), 2450–2463. https://doi.org/10.1109/TSMC.2021.3050183

Li, R., Wang, B., Zhang, T., & Sugi, T. (2023). A developed LSTM-ladder-network-based model for sleep stage classification. *IEEE Transactions on Neural Systems and Rehabilitation Engineering: a Publication of the IEEE Engineering in Medicine and Biology Society*, *31*, 1418–1428. https://doi.org/10.1109/TNSRE.2023.3246478

Lili, C., Wei, G., Zhen, J., & Gui-Quan, S. (2022). Sparse optimal control of pattern formations for an SIR reaction-diffusion epidemic model. *SIAM Journal on Applied Mathematics*, *82*(5), 1764–1790.

Lin, D., Liao, X., Dong, L., Yang, R., Yu, S. S., Iu, H. H.-C., Fernando, T., & Li, Z. (2021). Experimental study of fractional-order RC circuit model using the Caputo and Caputo-Fabrizio derivatives. *IEEE Transactions on Circuits and Systems I: Regular Papers*, *68*(3), 1034–1044. regular papers, https://doi.org/10.1109/TCSI.2020.3040556

Liu, S., Liu, C., Zhao, H., Liu, Y., & Dong, Z. (2022). Improved flux weakening control strategy for five-phase PMSM considering harmonic voltage vectors. *IEEE Transactions on Power Electronics*, *37*(9), 10967–10980. https://doi.org/10.1109/TPEL.2022.3164047

Luo, T., Xu, D., Cao, Z., Zhao, P., Wang, J., & Zhang, Q. (2024). Modeling the coupling propagation of information, behavior, and disease in multilayer heterogeneous networks. *IEEE Transactions on Computational Social Systems*, *11*(3), 4058–4070. https://doi.org/10.1109/TCSS.2023.3306014

Kamal, M., Amin, M.A., Ahmed, M., Ahmed, P. & Islam, M.A. (2025). Mathematical modeling and optimal control of social media addiction with stability and sensitivity analysis. *Franklin Open*, *12*, 1–16. doi: 10.1016/j.fraope.2025.100354.

Ma, X., Sun, G., Wang, Z., Chu, Y., Jin, Z., & Li, B. (2022). Transmission dynamics of brucellosis in jilin province, China: Effects of different control measures. *Communications in Nonlinear Science and Numerical Simulation*, *114*, 106702. https://doi.org/10.1016/j.cnsns.2022.106702

Mahapatra, D. P., & Triambak, S. (2022). Towards predicting COVID-19 infection waves: A random-walk Monte Carlo simulation approach. *Chaos, Solitons, and Fractals*, *156*, 111785. https://doi.org/10.1016/j.chaos.2021.111785]

Mengcan, M., Xiaofang, C., & Yongfang, X. (2021). Constrained voting extreme learning machine and its application. *Journal of Systems Engineering and Electronics*, *32*(1), 209–219. https://doi.org/10.23919/JSEE.2021.000018

Miao, Y., Wang, X., Wang, S., & Li, R. (2023). Adaptive switching control based on dynamic zero-moment point for versatile hip exoskeleton under hybrid locomotion. *IEEE Transactions on Industrial Electronics*, *70*(11), 11443–11452. https://doi.org/10.1109/TIE.2022.3229343

Naceri, A., Elsner, J., Trobinger, M., Sadeghian, H., Johannsmeier, L., Voigt, F., Chen, X., Macari, D., Jahne, C., Berlet, M., Fuchtmann, J., Figueredo, L., Feusner, H., Wilhelm, D., & Haddadin, S. (2022). Tactile robotic telemedicine for safe remote diagnostics in times of corona: system design, feasibility and usability study. *IEEE Robotics and Automation Letters*, *7*(4), 10296–10303. https://doi.org/10.1109/LRA.2022.3191563

Okafor, K. C., & Longe, O. M. (2022). Smart deployment of IoT-TelosB service care StreamRobot using software-defined reliability optimisation design. *Heliyon*, *8* (6), e09634. https://doi.org/10.1016/j.heliyon.2022.e09634

Okafor, K. C., et al. (2025). HAC-19: A co-infection model for infectious diseases using iot-networked robots. *IEEE Internet of Things Journal*, *12*(16), 33545–33560. https://doi.org/10.1109/JIOT.2025.3575273

Oyelade, O. N., Ezugwu, A. E.-S., & Chiroma, H. (2021). CovFrameNet: An enhanced deep learning framework for COVID-19 detection. *IEEE Access: practical Innovations, Open Solutions*, *9*, 77905–77919. https://doi.org/10.1109/ACCESS.2021.3083516

Phogat, K. S., Chatterjee, D., & Banavar, R. N. (2018). A discrete-time Pontryagin maximum principle on matrix lie groups. *Automatica*, *97*, 376–391. https://doi.org/10.1016/j.automatica.2018.08.026

Qasem, O., Davari, M., Gao, W., Kirk, D. R., & Chai, T. (2024). Hybrid iteration ADP algorithm to solve cooperative, optimal output regulation problem for continuous-time, linear, multiagent systems: theory and application in islanded modern microgrids with IBRs. *IEEE Transactions on Industrial Electronics*, *71*(1), 834–845. https://doi.org/10.1109/TIE.2023.3247734

Rey, A. S. E., Olive, R. C., Bryan, S. H., Renier, G. M., Victoria, M. P. M., Rhudaina, Z. M., Carlene, P. C. P., Pamela, K. N. S., Fatima, L. E. S., Polly, W. S., Thomas, H. M. V., & A. de los Reyes, A. (2023). A model-based strategy for the COVID-19 vaccine roll-out in the Philippines. *Journal of Theoretical Biology*, *573*, 1–17. https://doi.org/10.1016/j.jtbi.2023.111596

Richard, Q., Alizon, S., Choisy, M., Sofonea, M. T., & Djidjou-Demasse, R. (2021). Age-structured non-pharmaceutical interventions for optimal control of COVID-19 epidemic. *PLoS Comput. Biol., 17*(3), 1–25. doi: 10.1371/journal.pcbi.1008776.

Rossetti, N., Gerevini, A. E., Olivato, M., Putelli, L., Chiari, M., Serina, I., Minisci, D., & Foca, E. (2023). Recurrent neural networks for daily estimation of COVID-19 prognosis with uncertainty handling. *Procedia Computer Science*, *225*, 1542–1551. https://doi.org/10.1016/j.procs.2023.10.143

Salwahan, S., Abbas, S., & Tridane, A. (2025). Optimal control of a periodically switched epidemic model. *International Journal of Dynamics and Control*, *13*(2), 98. https://doi.org/10.1007/s40435-025-01600-1

Shastri, S., Singh, K., Kumar, S., Kour, P., & Mansotra, V. (2020). Time series forecasting of Covid-19 using deep learning models: India-USA comparative case study. *Chaos, Solitons, and Fractals*, *140*, 110227. https://doi.org/10.1016/j.chaos.2020.110227

Sivadas, N. A., Panda, P., & Mahajan, A. (2023). Control strategies for the COVID-19 infection wave in India: A mathematical model incorporating vaccine effectiveness,. *IEEE Transactions on Computational Social Systems*, *10*(6), 3262–3272. https://doi.org/10.1109/TCSS.2022.3210404

Soulaimani, S., & Kaddar, A. (2023). Analysis and optimal control of a fractional order SEIR epidemic model with general incidence and vaccination,. *IEEE Access*, *11*, 81995–82002. https://doi.org/10.1109/ACCESS.2023.3300456

Stewart, G., Heusden, K., & Dumont, G. A. (2020). "How control theory can help us control Covid-19. *inIEEE Spectrum*, *57*(6), 22–29. https://doi.org/10.1109/MSPEC.2020.9099929

Sun, J., Yuan, K., Chen, C., Xu, H., Wang, H., Zhi, Y., Peng, S., Peng, C., Huang, N., Huang, G., & Yang, A. (2023). Causality network of infectious disease revealed with causal decomposition. *IEEE Journal of Biomedical and Health Informatics*, *27*(7), 3657–3665. https://doi.org/10.1109/JBHI.2023.3268081

Tchoumi, S. Y., Diagne, M. L., Rwezaura, H., & Tchuenche, J. M. (2021). Malaria and COVID-19 co-dynamics: A mathematical model and optimal control. *Applied Mathematical Modelling*, *99*, 294–327. https://doi.org/10.1016/j.apm.2021.06.016

Tiago, C., Snare, S. R., Šprem, J., & McLeod, K. (2023). A domain translation framework with an adversarial denoising diffusion model to generate synthetic datasets of Echocardiography images. *IEEE Access*, *11*, 17594–17602. https://doi.org/10.1109/ACCESS.2023.3246762

U.K. Parliament. Commons Library. (2023). UK shipping industry statistics. Commons Library Research Briefing, CBP-9309. https://commonslibrary.parliament.uk/research-briefings/cbp-9309/.

U.K. Parliament. Commons Library. (2023). *UK shipping industry statistics*. Commons Library Research Briefing. CBP-9309, 7 Aug. [Online].

U.S. Government Accountability Office. (2023). Federal electric vehicle efforts: Vehicle purchasing goals have been set, but additional steps are needed to achieve goals [Online]. GAO-23-106647. https://www.gao.gov/products/gao-23-106647

Wang, L., She, A., & Xie, Y. (2023). The dynamics analysis of Gompertz virus disease model under impulsive control. *Scientific Reports*, *13*(1), 10180. https://doi.org/10.1038/s41598-023-37205-x

Wang, Q., Tian, Y., Du, X., Ko, H., Ip, B. Y. M., Leung, T. W. H., Yu, S. C. H., & Zhang, L. Oct (2022). Magnetic navigation of collective cell microrobots in blood under ultrasound doppler imaging. *IEEE/ASME Transactions on Mechatronics*, *27*(5), 3174–3185. https://doi.org/10.1109/TMECH.2021.3109346

Yang, J., Yang, L., & Jin, Z. (2023). Optimal strategies of the age-specific vaccination and antiviral treatment against influenza. *Chaos, Solitons & Fractals*, *168*, 113199. https://doi.org/10.1016/j.chaos.2023.113199

Yin, J. J., Tang, W., & Man, K. F. (2007). Identification of biological neural network using jumping gene genetic algorithm [Paper presentation]. IECON 2007 – 33rd Annual Conference of the IEEE Industrial Electronics Society, Taipei, Taiwan. pp. 693–697. https://doi.org/10.1109/IECON.2007.4460066

Yousri, D., Mudhsh, M., Shaker, Y. O., Abualigah, L., Tag-Eldin, E., Abd Elaziz, M., & Allam, D. (2022). Modified interactive algorithm based on Runge Kutta optimizer for photovoltaic modeling: justification under partial shading and varied temperature conditions. *IEEE Access*, *10*, 20793–20815., https://doi.org/10.1109/ACCESS.2022.3152160

Zaman, G., Kang, Y. H., & Jung, I. H. (2008). Stability and optimal vaccination of an SIR epidemicmodel. *Bio Systems*, *93*(3), 240–249. https://doi.org/10.1016/j.biosystems.2008.05.004

Zaman, G., Kang, Y. H., & Jung, I. H. (2009). Optimal treatment of an SIR epidemic model with time delay. *Bio Systems*, *98*(1), 43–50. https://doi.org/10.1016/j.biosystems.2009.05.006

Zaman, G., Kang, Y. H., Cho, G., & Jung, I. H. (2017). Optimal strategy of vaccination & treatment in an SIR epidemic model. *Mathematics and Computers in Simulation*, *136*, 63–77. https://doi.org/10.1016/j.matcom.2016.11.010

Zhai, J., & Xu, G. (2021). A novel non-singular terminal sliding mode trajectory tracking control for robotic manipulators,. *IEEE Transactions on Circuits and Systems II: Express Briefs*, *68*(1), 391–395. https://doi.org/10.1109/TCSII.2020.2999937

Zhang, X., Pan, W., Scattolini, R., Yu, S., & Xu, X. (2022). Robust tube-based model predictive control with Koopman operators. *Automatica*, *137,* 1-10. https://doi.org/10.1016/j.automatica.2021.110114